Abstract

Title of Dissertation: γ -Ray Studies of Stellar Graveyards: *Fermi*-LAT Observations of Supernova Remnants and Spatially Extended Emission

Jamie Michael Cohen, Doctor of Philosophy, 2016

Dissertation directed by: Doctor Elizabeth Hays
Astroparticle Physics Laboratory, Code 661
NASA Goddard Space Flight Center

Professor M. Coleman Miller
Department of Astronomy
University of Maryland

Here I shall abstract!

γ -Ray Studies of Stellar Graveyards: *Fermi*-LAT Observations of Supernova Remnants and Spatially Extended Emission

by

Jamie Michael Cohen

Dissertation submitted to the Faculty of the Graduate School of the
University of Maryland at College Park in partial fulfillment
of the requirements for the degree of
Doctor of Philosophy
2016

Advisory Committee:

Doctor Elizabeth Hays, Advisor
Professor M. Coleman Miller, Chair/Advisor
Professor Christopher S. Reynolds
Professor Derek C. Richardson
Professor Jordan Goodman, Dean's Representative

Preface

This thesis consists of 8 chapters [JAM: 9 if I have time thrown in other work I've done like SNR-MC, above 10 GeV] including an introduction, conclusion and three background chapters on supernova remnants, γ-ray emission theory and detection methods, and a description of the relevant aspects of the *Fermi* Gamma Ray Space Telescope.

Chapters 5 and 6 are, respectively, taken in part from "The First *Fermi*-LAT Supernova Remnant Catalog"and "'2FHL: The Second Catalog of Hard Fermi-LAT Sources", both published in *The Astrophysical Journal Supplement* in 2016. Both papers are large, catalog studies involving the entire LAT collaboration. The parts of those papers included in this dissertation are the those in which I had direct involvement (analysis, writing, discussion). The text in Chapters 5 and 6 also expands on the work I did for those papers, and provides further detail on analysis not included in the papers.

Chapter 7 is the contents of a paper currently in preparation and under LAT team internal review. The title of this paper is to be "*Fermi*-LAT Observations of Extended Gamma-Ray Emission in the Direction of SNR G150.3+4.5" (Cohen et al. 2016) [JAM: to be published in?]. The contents of the paper is included in entirety in this thesis, including additional supplementary material not to be included in the journal article.

To Vanessa ♡

Acknowledgements

I should probably thank someone because I'm not a degenerate.

Contents

List of Tables

List of Figures

Chapter 1

Introduction

"Maybe I'll have a super relevant quote here!"

—by some awesome human, from *Some book*

1.1 Goooo γ-rays go!

In this thesis we...or should I start with the extreme environs line?

Overview of the entire thesis, why gamma-rays, why the Large Area Telescope (LAT), why SNRand pulsar wind nebula (PWN)and extended sources.

Higher energy studies with the LAT have been my focus since the beginning. Talk about what's nice about staying above 1 GeV, 10 GeV, 50 GeV.

GeV TeV connection for 2FHL

Radio GeV for SNR cat (traces same particle population)

The advent of the LATpresents for the first time the capability to spectrally and spatially resolve SNR at GeVenergies.

it is uniquely situated to address these issues

egret was mostly pointed observation instrumented that would sometimes dwell

on a spot for a couple of weeks, had a smaller field o view, didn't get as many photons (the LAT saw the entire EGRET sky in some short amount of time)

SNRsas sources of relativistic particles

Despite being the prime energy range to observe the effects of cosmic particle acceleration, the photon spectral energy distribution (SED) resulting from these overlapping emission channels are often difficult to spectrally distinguish from one another. [JAM: what's the point of this last sentence here? maybe no need to mention this now, i really just want to motivate GeV energies]

when talking about Energetic Gamma-Ray Experiment Telescope (EGRET)

With its unprecedented sensitivity and angular resolution above 1 GeV, the LAT provides for the first time the opportunity to distinguish SNR-emitted photons from their backgrounds, and to unambiguously detect and identify dozens of SNRs. [JAM: maybe this is for the intro/abstract because it's a little vague]

The LAT is uniquely situated to address these goals and definitively detect and identify dozens SNRs

Thompson et al. (1993) gives the 68% containment radius as $\theta \leq 5.85^{\circ}(E_{\gamma}/100\,\mathrm{MeV})^{-0.534}$

1.2 I Think I Hate Most of the Section Titles :(

1.3 Maybe None of the Chapters Need Introductions?

1.4 Dissertation Overview

Chapter 2

Supernova Remnants: Theory and Observation

2.1 Introduction

Why study SNRs, what they are, history of SNR, radio detections,

2.2 Formation and Evolution

-Stars die and explode, that energy is very quickly put into the surroundings

-snowplough, ST, radiative,

- what else?

How we detect gamma-rays from SNRs/PWNe in the Galaxy leads to and analysis section maybe?

2.3 Morphology and Classification

SNRs characterized by morphology and evolution properties

shell type, mixed morphology, filled center composite)

Since I eventually do these all plane surveys, what does the spatial distribution of them at radio look like?

Not sure how much to say about radio observations, x-ray, TeV

2.4 Cosmic Ray SNR connection

Give the whole, if 10% of energy of SN explosion goes into particle acceleration, we can explain cosmic rays

Particle acceleration and DSA

This leads to gamma-ray section

2.5 Summary

In this section we summarized the end phase of stellar evolution (just enough to motivate SNRs) and descried the environs surrounding the supernova; development and phases of SNRs (and PWNe?). In particular we detailed the nonthermal emission mechanisms that produce γ -ray radiation, detection of young vs middle-aged(evolved, interacting with surroundings/dense medium),TeV detects younger typically, the troubles of detecting extension from them(?) something about different emission zones? Troubles disentangling hadronic from leptonic at γ -rays. γ -ray spectral and morphological features. Trends across the population wrt spectral shape/breaks, higher luminosity for interacting rems. Cosmic rays, using gamma-rays to probe CR population. So much of γ -ray astro is really about studying CRs,

how much to say about them?

2.6 Scratch

This chapter needs a different title. It's more focused on the specific sources being studied in this thesis. Galactic extended sources, SNRs, PWNe, but as in the SNRcat, not just extended SNRs, point-like SNRs as well.

Less focus on PWNe. Only give as much as I feel I need to support mentioning them a bit for 2FHL?

The focus of this section is supernova remnants in a gamma-ray context. Theory of evolution, what the gamma-ray emission is like, what we can learn from them individually. This leads to the 1st SNR cat section for what we can do with them ensemble

NOt sure I really need any PWN stuff yet

in 2FHL we detect some pwn. If including above 10gev work, they'll be there too. Much of the thesis is really about extended gamma-ray sources, but not sure how that fits into the title and chapters yet

Do I need to get into composite SNRs (composite means SNR + PWN) Maybe relevant for G150? Some things about interaction of reverse shock with PWN and crushing/reverberations of the PWN?

Montmerle (1979)

Chapter 3

Gamma-ray Astronomy

3.1 Introduction

Maybe this is not just gamma astro, but gamma astro of SNRS

The story of γ-ray's from astrophysical objects is a tale of the most extreme, energetic, and violent environments in our universe. Discovered by Paul Villard studying radiation from radium and named by Ernest Rutherford, who previously uncovered the nature of α and β radiation, γ-ray's are the highest named energy of light

more historical context instead of a separate section

what is a gamma-ray

why bother studying gamma-rays

probe of extreme environments

thermal means follows maxwellian (maxwell-Boltzman) distribution

[JAM: snrs as source of Galactic cosmic rays, and thus as drivers of Galactic evolution]

3.2 γ-ray Emission Mechanisms

Gamma-rays as a probe of cosmic rays and cosmic acceleration processes

gamma-ray astronomy as a proxy for studying cosmic rays and acceleration/diffusion processes. How much to get into CR.

Cosmic particle accelerators and γ-ray's accelerator plus target often

What's a CR, quick, general CR properties that are relevant to SNRs

why use gamma's to study CR

gamma-ray production mechanisms

myriad of gamma-ray generating mechanisms operate at this energy, so it's sometimes the only range that we can observe this emission in:

-Synch, -Bremss, -IC, -pi0,

3.3 Sources of γ-ray's

Maybe don't need this? The reason to is to say SNRs early on. Would I mention other sources to be complete?

SNRs as the primary source of Galactic CRs, order of mag (zwicky?) energy from 0.1*E SNR could account for energy in CRs in Galaxy

3.4 γ-ray Detection

Quick rehash of method of detecting γ-ray's? Or is this just about previous γ-ray detectors and the state of the γ-ray sky pre-Fermi? mention telescopes up to EGRET, bit of detail on EGRET and what the pre-Fermi γ-ray sky looked like, in particular in the context of SNRs, PWN, Galactic plane

gamma-ray telescopes leads into the LAT, Egret was predecessor , what it did and what were some relevant unanswered questions regarding supernova remnants

One of the primary goals of fermi was to identify these sources and the site of CR acceleration. But also to uniquely open this high energy window that where no other telescopes really operated Brief history of radio detection of SNRs. detection at other wavelengths. what we see at γ -rays?

Motivation for why to study them (Sturner & Dermer 1995) (Esposito et al. 1996)

3.5 Scratch

Altho' many miles from bomb zero, Dr. Bruce Banner is bathed in the full force of the mysterious Gamma Rays!

Chapter 4

The *Fermi* Gamma-Ray Space Telescope and γ-ray Data Analysis

4.1 Introduction

The *Fermi* Gamma-Ray Space Telescope (*Fermi* hereafter), successor to the EGRET instrument on Compton Gamma-Ray Observatory (CGRO), was successfully launched into orbit around Earth on June 11 2008. *Fermi* consists of two instruments, the LAT and the Gamma-ray Burst Monitor (GBM).

The LAT, which is the primary instrument on *Fermi*, is a pair conversion telescope designed to detect photons from 20 MeV to greater than 1 TeV. Its standard mode of operation is a sky-survey mode in which it observes the entire sky every 3 hours. The GBM is designed to detect gamma-ray bursts (GRBs) in a waveband overlapping that of the LAT, and complementary in lowering that energy range. It is comprised of two types of scintillator detectors: two bismuth germanate crystals that operate from 150 keV to 30 MeV, and 12 sodium iodide crystals sensitive to photons between 8 keV and 1 MeV.

Combined the LAT and GBM make up a formidable observatory, spanning more than 8 decades in energy, and is currently the only instrument performing all-sky observation in this broad energy range. [JAM: maybe I don't need any gbm stuff? I mentioned it just to be complete about what fermi is, probably won't mention it again, and this last par doesn't really flow into the next]

4.2 The Large Area Telescope

The need for Fermi in the context of what EGRET did

What were open questions from EGRET era, state of γ-ray detection of SNRs, what question was Fermi deigned to answe

Description of the instrument [JAM: not sure this really goes here, separate section for what questions Fermi was designed to answer?]

track and reconstruct the path of Describe it's objectives and strengths over predecessors Details on the LAT and it's design, be sure to focus on things that particularly pertinent to the work I've done like what determines the PSF, thing about Pass 8 here maybe? Or maybe later on.

what science was it designed to answer

general capabilities

details about aspect of the LAT related to extended sources, what determines PSF

4.3 γ-ray Data Analysis

Why maximum likelihood, how it's formulated, implemented in the Science Tools, pointlike and the analysis for extended sources. Diffuse emission.

Four steps to going from observing the sky to final LAT analysis:

Instrument taking data: How we get to counts

Reconstruction : How we get photons

Likelihood: How to characterize sky using response functions, point source and diffuse modeling

Likelihood for ES: how to use likelihood methods to char and resolve sources measure extension

Section on diffuse emission

4.3.1 Do I need subsections?

4.4 Scratch

[JAM: Fermi goals: 1. Resolve the γ-ray sky: the origins of diffuse emission and the nature of unidentified sources: Source identification through good source localization, measurement of spectra across broad energy range, nearly continuous monitoring of the sky for temporal variability 2. Understand the mechanisms of particle acceleration in celestial sources] I'm not sure about this chapter yet. Maybe it's a general section on Analysis of Fermi data,

Chapter 5

Revealing the GeV Supernova Remnant Population: The First *Fermi*-LAT Supernova Remnant Catalog

5.1 Supernova Remnants at γ-ray Energies

By the end of the its science run, EGRET had detected 271 sources above 100 MeV, within a minimum detection significance of 4σ, 170 of which had no clear multi-wavelength counterpart, with 81 of those unidentified lying within $|b| < 10^{\circ}$ of the Galactic plane (Hartman et al. 1999). The main hindrances to source identification were the numerous potential source counterparts (the EGRET point spread function (PSF) was energy dependent, with a 68% containment radius of $\sim 6^{\circ}$ at 100 MeV and smaller for higher energies) and the large EGRET error boxes. In addition to this, the primary method for identifying a γ-ray source as an SNR is

through a compatible angular extent with observations at some other wavelength, thus the ability to resolve emission from an SNR is vital to understanding the mechanisms therein giving rise to γ-rays. Figure 5.1 shows an EGRET all-sky map at $E > 100$ MeV where the preponderance of unidentified sources and locations thereof are made clear.

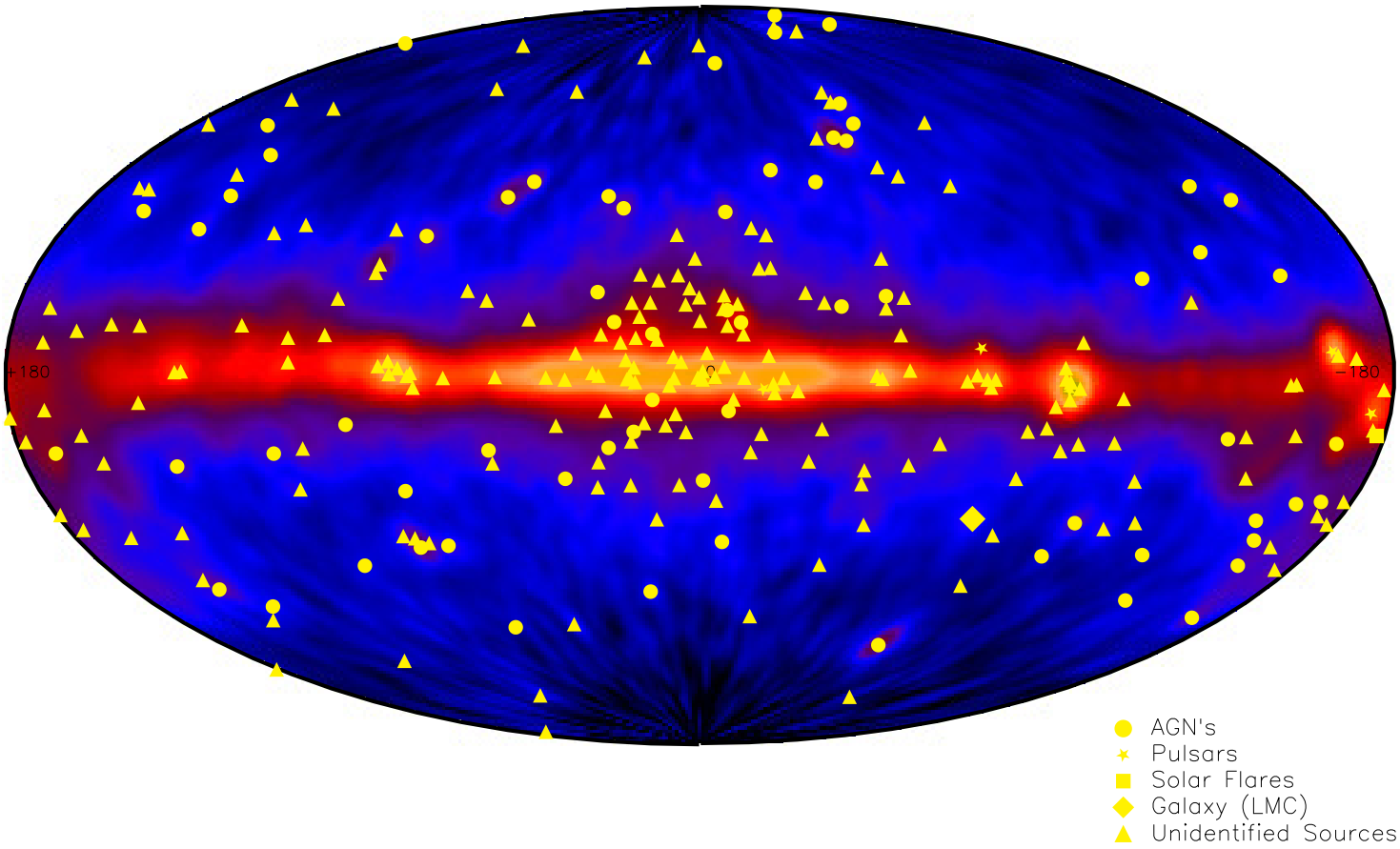

Figure 5.1: Third EGRET catalog all-sky map. Unidentified sources represented by triangles. Image courtesy of `https://heasarc.gsfc.nasa.gov/docs/cgro/images/epo/gallery/skymaps/`

In spite of the difficulties in EGRET source association, many studies have attempted correlating the unidentified EGRET sources with various Galactic populations. In particular, several authors found strong evidence for statistical correlation between SNRs and some of the low-latitude unidentified sources (Esposito et al.

1996; Romero et al. 1999; Sturner & Dermer 1995). In a review of the state of potential SNR / EGRET associations, Torres et al. (2003) showed that there were 19 unidentified EGRET sources that had an SNR fall within its 95% error box. Performing Monte Carlo simulations of the population of EGRET sources, they determined that the chance probability for the 19 sources to be coincident with an SNR was 1.05×10^{-5}, implying a probability of 0.99998 that at least one of the associations is real. Despite the statistical correlation of EGRET sources with SNRs, there were no definitive associations of an SNR with any EGRET sources.

As the successor to EGRET, the LAT was designed to improve upon its predecessor in a multitude of areas relevant to detecting SNRs (Ackermann et al. 2012c; Atwood et al. 2009). The LAT has a much improved angular resolution (68% single-photon containment radius $\sim 0.4^\circ$ at 1 GeV for photons with the best quality direction reconstruction, PSF3 event type, compared to $\sim 1.7^\circ$ for EGRET at the same energy), necessary to resolve SNRs as extended objects. The LAT also benefits from a superior sensitivity due to a combination of the improved PSF, larger peak effective area (> 9000 cm^2 vs. ~ 1500 cm^2), wider field of view (FoV) (2.4 sr, which is nearly 5 times that of EGRET), and deeper, more-uniform sky exposure (afforded by the LAT's scanning observations as opposed to EGRET's pointing operation).

This bump in sensitivity results in the LAT detecting considerably more sources than EGRET. Remarkably, within its first three months of commission, the LAT detected 205 sources above 10σ significance (Abdo 2009), and by 11 months, 1451 sources above 4σ (Abdo et al. 2010a), compared to the aforementioned 271 over the entire EGRET mission. In fact, over its lifetime, EGRET detected a total of about 1.5 x 10^6 cosmic photons (Thompson et al. 1993), while as of March 2016, the LAT has detected $\sim$ 863 x 10^6 [JAM: change this number in June] source class photons. The LAT's point-source sensitivity peaks between 1 and 10 GeV, depending on

location on the sky. [JAM: plot comparing lat to egret sensitivity?]. With its increased sensitivity and higher energy range (up to $\sim$ 2 TeV with the recent Pass 8 event reconstruction improvements, which is nearly an order of magnitude higher than EGRET), the LAT is uniquely situated to study the γ-ray morphology and spectra of SNRs.

Both energetic lepton interactions (i.e.inverse compton (IC) radiation of relativistic electrons interacting with ambient photon fields, and nonthermal bremsstrahlung) and hadronic processes (π_0 decay γ-rays from cosmic ray (CR) protons encountering surrounding nuclei) produce spectra observable at γ-ray energies (see Chapter 3 for details). While the IC generating electron population is also observable through emission of radio synchrotron photons, the proton-proton interaction solely emits γ-rays. Despite being the prime energy range to observe the effects of cosmic particle acceleration, complexities at the lower LAT energy range stymie SNR morphology studies.

The LAT detects a strong, soft band of diffuse emission in the Galactic plane due to the interactions of CRs with interstellar material. This bright diffuse radiation combined with the multiple potential emission scenarios, broadening PSF at decreasing energy, and a high source density in the plane can make it difficult to spatially disentangle sources observed by the LAT. To circumvent these difficulties, the majority of the analyses undertaken in this thesis are focused on the E $\geq$ 1 GeV energy range. This energy band is ideal for probing the properties of the accelerated particle populations present in the SNR environment. Studies of SNRs above 1 GeV benefit from finer LAT PSF, striking a balance between minimizing the diffuse contribution, maximizing photon sensitivity, and retaining good photon statistics. Furthermore, evolved SNRs exhibit a spectral break between 1-10 GeV (Hewitt & Lemoine-Goumard 2015). Explanations for the break range from Alfvén wave

evanescence generated by collisions of partially ionized material in molecular clouds (MCs) overtaken by SNR shocks (Malkov et al. 2011), reflected shocks in clouds Inoue et al. (2010), and energy-dependent diffusion from shocks Ohira et al. (2011). Studying SNRs in this energy range hones our capability to tackle several goals set out by the *Fermi* team when the mission was conceived.

Two of the primary science goals of the LAT are to 1. resolve the γ-ray sky, uncovering the nature of the unidentified sources detected by EGRET, and 2. to understand the mechanisms of cosmic particle acceleration (Atwood et al. 2009). In this chapter, we describe our efforts towards addressing these questions by studying the γ-ray emission coincident with sources comprising the population of known radio emitting SNRs.

Prior to this work, several individual studies with the LAT had successfully resolved spatially extended emission from SNRs (Acero et al. 2015, and references therein), yet no systematic analysis leveraging the LAT's full-sky coverage had thus been attempted. We performed for the first time a uniform study of the SNRs in aggregate to measure the properties common to these objects. An understanding of these common characteristics allows us to assess SNRs as a class of γ-ray and CR emitting objects and serves as the impetus for this uniform analysis of the known Galactic SNRs. We report here on the published results from the First *Fermi*-LAT Supernova Remnant Catalog (SNRcat) (Acero et al. 2016).

[JAM: 2FGL only had 7 ID'd SNR, 4 snr, 58 spp. 3FGL had 12 SNR, 11 snr, 49 spp. I'm not sure what made some snr vs. spp. They must have all been point sources right? No known radio pwn, psr?]

5.2 The `pointlike` Maximum-Likelihood Package and `addSrcs`

As described in Chapter 4, maximum-likelihood analysis is the ideal method for determining the properties of LAT-observed sources due to the "counting-experiment" nature of *Fermi*-LAT. The standard maximum-likelihood tools for analyzing LAT data are implemented via the *Fermi* Science Tools, and in particular `gtlike`. Despite being the optimum method, likelihood analysis of LAT data is complex due to the highly non-linear performance of the instrument and can be computationally expensive. It is necessary to manage the data and response of the telescope as well as the source and background models. Furthermore, due to the broadening of the PSF at low energies, even when studying a single source, it is necessary to include in the model descriptions of multiple surrounding sources. The `pointlike` binned maximum likelihood package was created to ameliorate some of these issues. Described in detail in Kerr (2010), `pointlike` is an alternate likelihood analysis framework (a collection of Python modules with additional wrappers for accessing C++ code), designed to be interactive and rapidly evaluate likelihoods.

There are several ways in which `pointlike` improves in efficiency compared to the Science Tools. It saves computational time, while sacrificing some accuracy, with several assumptions and approximations, such as the PSF not varying strongly with photon incidence angle (allowing a single PSF for each individual bin), and sources having a steady flux in individual short time bins. Most importantly though, `pointlike` varies the size of spatially binned `HEALPix` pixels (Górski et al. 2005) according to energy. The PSF at lower energies is large and each energy bin can contain multiple counts, while at higher energies, the PSF shrinks and many pixels will not contain even a single count. `pointlike` creates `HEALPix` bins that are

approximately the size of the PSF at a given energy, and disregards empty bins to speed up the likelihood calculation.

In addition to these computational, time saving efficiencies, tools to analyze spatially extended sources have also been built into the `pointlike` framework. Studying the position and extension of an extended source, while possible with the standard *Fermi* Science Tools, is a cumbersome process. `gtlike` is not capable of simultaneously maximizing the likelihood of a source's spectral and spatial parameters, so to assess the morphology of a source, an iterative process of fitting a spatially fixed source's spectrum and then varying the sources centroid and extension is required. To address the issues that arise when studying individual extended sources, Lande et al. (2012) developed and validated spatial likelihood fitting tools for `pointlike`, taking advantage of the time-saving properties built therein.

To fit the position and extension of a source, `pointlike` assumes that the spatial and spectral distribution of a source's expected photon distribution are separable. The extended source's shape is convolved with the LAT PSF (which is a function of energy) to determine the expected distribution. Then, the `minuit` numerical minimization library(James & Roos 1975) is used to maximize the likelihood of the model by simultaneously varying the spectrum, extension, and position of the source. Various geometric surface brightness models are built into `pointlike`, including, but not limited to a uniform intensity disk and ring, and a 2D Gaussian, with radially and non-radially symmetric versions of each. Akin to the speed optimizations mentioned previously, for radially symmetric sources, `pointlike` calculates the angular integral of a source's expected photon distributions analytically to save computational time.

The significance of extension of a source is determined by using the likelihood ratio test (LRT). The LRT is a statistical method to assess the goodness-of-fit of two different models. The likelihood (as described in Chapter §4.3[JAM: do this,

reference cash,mattox, fisher for first use of word likelihood?]) is calculated for two models, one of which can be reduced to the other hypothesis under certain conditions. If the more complex model can be reduced to the simpler model (called the null hypothesis), we say the simpler hypothesis is nested within the more complex. In the LRT, the test statistic (TS) is defined as:

$$\mathrm{TS} \equiv 2 \log(\ \mathcal{L}(\mathrm{H}_1)\ /\ \mathcal{L}(\mathrm{H}_0)), \tag{5.1}$$

with H_1 being the more complex hypothesis and H_0 the null. Applying this to the hypothesis of a spatially extended source, we can calculate the significance of a source being extended compared to that of the source being modeled as point source as:

$$\mathrm{TS}_{\mathrm{ext}} \equiv 2 \log(\ \mathcal{L}_{\mathrm{es}}\ /\ \mathcal{L}_{\mathrm{ps}}) = \mathrm{TS}_{\mathrm{es}} - \mathrm{TS}_{\mathrm{ps}}, \tag{5.2}$$

Mattox et al. (1996) detail how by Wilk's theorem, the TS for detection of a point source (with the null hypothesis being that with no source present, or 0 flux) should be distributed as a chi-squared distribution in the null hypothesis for an increasing sample size, which for photon counting experiments, is the number of events relevant to the parameter being estimated. Specifically,

$$\mathrm{PDF}(\mathrm{TS}) = 1/2\ \chi^2_1, \tag{5.3}$$

where PDF(TS) is the probability distribution function for obtaining a specific value of TS and χ^2_1 is the chi-squared distribution for one degrees of freedom. The factor of 1/2 arises from the fact that the flux of a source is not permitted to be zero, and since negative and positive fluctuations in a parameter's value contribute equally to the TS, half of the distribution is lost with the positive flux restriction. The significance of detection is oft quoted as $\sigma \approx \sqrt{\mathrm{TS}}$, which is strictly valid only

for χ^2_1. More generally, when comparing the likelihood of two models with n degrees of freedom between them, equation 5.3 applies, but using χ^2_n for n degrees of freedom versus one.

Lande et al. (2012), extended (and verified) this definition of TS to calculating the significance of extension, replacing the source flux with its radius. The uncertainty of the extension parameter is estimated by fixing a source's position while varying the extension until the log likelihood decreases by 1/2 from the maximum value (i.e. 1σ errors). [JAM: use that TS vs extension figure I didn't include in the G150 paper to demonstrate where the TS drops by half from the peak?] A similar procedure is used to estimate the errors on a source's position, but rather, fixing the extension and spectrum (Nolan et al. 2012). While `pointlike` is an tool for the analyses described above, `gtlike` is still the go-to for estimating the best-fit spectral parameters since it is expected to be slightly more accurate than `pointlike` since it makes approximations. For the studies in this thesis, we used `pointlike` to calculate extension and source positions, and then use the `pointlike` results as a starting point for the likelihood parameter estimation of spectra with `gtlike`.

With its efficient likelihood calculations, and ability to simultaneously fit both the spectral and spatial parameters of a source, `pointlike` is ideally suited for large-scale studies (like the all-sky analyses performed for the LAT point source catalogs), and analyses requiring several iterations. Studying the γ-ray emission from the population of Galactic SNRs is precisely the sort of analysis that `pointlike` was designed to perform. To attain the best understanding of a source of interest, the best characterization of the corresponding RoI is necessary. In particular, to understand the GeV emission from a potentially extended SNR, it is important to quantify the surrounding emission because of the steep energy-dependence of the LAT PSF. This can be especially challenging in dense source and strong diffuse-

dominated regions, like the Galactic plane where the SNRs we are studying lie. We have developed an automated method for systematically locating and modeling all potential point and/or extended sources in an RoI using `pointlike`.

A typical LAT analysis starts by including all sources from the most recent LAT point source catalog and modifying the RoI to suit ones needs. Unmodeled emission car arise if using a dataset longer than that used in the most recent catalog or by focusing on a different energy range compared to that of the catalogs. We created a Python subclass of the primary `pointlike` analysis object (which works within that framework, inheriting all of the class' features, while adding new functionality) to systematically and uniformly characterize sources in an RoI by finding residual, unmodeled emission in the region and iteratively add sources to the RoI to account for this emission. The main module in the designed codebase was dubbed `addSrcs`.

The general work flow of `addSrcs` is to start with a model of the RoI, including some combination of the diffuse background components, point and extended sources. `addSrcs` reads in a residual TS map or creates one on the fly if none is passed in. Residual emission is detected by finding the peak emission in the TS map and adding a source to the existing RoI at the position of the peak pixel. Either all point or extended sources can be iteratively detected and added to the RoI. For the SNRcat, we exclusively ran `addSrcs` in point source mode. Chapter 6.1 provides an application of `addSrcs` for extended sources.

In point source mode, a point source with a power law (PL) spectrum is added to the model of the region, a likelihood fit of the RoI is performed, and subsequently, the source's position is localized. Similarly, in extended mode a PL extended source (of any morphological form included in `pointlike`) is added to the RoI with a small seed radius, and the spatial parameters of the newly added source are fit simultaneously with the spectra of the other sources already in the model. If the source has

$TS_{ext} < 16$ (equivalent to a 4σ extension significance and validated through simulations in Lande et al. (2012) as a reasonable extension detection significance), the exteded source is replaced with a point source and the iteration continues as in point source mode. To extend the functionality of `addSrcs` and make it generally applicable to a multitude of LAT analyses, several optional methods were built in.

One such option is to test the newly added source for signs of spectral curvature (described further in Chapter **??**). If the source is found to show significant spectral curvature, the appropriate curved spectral model is retained, otherwise, we revert to the best-fit PL model. Another option provided is to fix the new sources spectrum if it is within a given angular separation of the center of the RoI to limit the number of free parameters for the likelihood fit and aid in proper convergence. If the source of interest being studied is not central in the RoI it might be beneficial to free the spectral parameters of sources within a given distance of the newly added source rather than from the center of the RoI. This choice was also built into `addSrcs`. Further, we included an option to refit the extension of any extended source already in the model at each iteration if they are within a given distance of the new (point or extended) source. Due to the broad size of the PSF, nearby source spectra can be influenced by each other, (particularly for extended sources) so the iterative procedure allows the likelihood to relax to a preferred value when adding new sources.

Throughout the `addSrcs` process, various checks are performed to ensure that parameter values are reasonable, the likelihood fit converges, and the procedure is generally running as expected. The range of permissible fit values for a parameter can be limited, the values of the parameters themselves can be fixed, or a consistently poorly-fit source can be automatically removed from the model. During the source localization step, if the fit goes awry and the source wanders too far from its initial

position, the position of the source can be rolled back to its staring location and fixed. Checks were also included to keep track of the Galactic diffuse and isotropic emission models to ensure they were adequately fit.

The penultimate step of the iteration is to produce various diagnostic plots and output information about the fits, the spectral and spatial parameters of each source in the model, and other relevant information such as the TS of the source and loglikelihood of the fit. Finally, a new residual TS map of the region is created and the source addition procedure repeats until a given threshold in TS is reached. The peak pixel TS found in the residual TS map does not necessarily decrease monotonically, as is expected of the actual TS of successive sources as more of the emission is accounted for and the model improved. Since the peak pixel TS can fluctuate a bit, to ensure that we do not miss significant sources in the RoI, we continue adding sources until the TS threshold is reached for some number of successive sources (discussed further in 5.6). After sources are no longer being added to the region, we iteratively remove souces with TS less than a given threshold (typically TS < 16, again see Chapter 5.6) starting with the lowest TS sources first. As each source is removed, we refit the RoI, including any extended sources close to the removed source. When the TS of all sources in the RoI are above threshold, we deem the emission in the RoI to be sufficiently characterized.

In the following sections, we detail the application of `addSrcs` to studying the GeV Galactic SNR population and describe the analysis and results presented in Acero et al. (2016).

[JAM: show some example region map with unmodeled sources and then the final result where sources were filled in? Extended vs not extended (just use 2FHL vs this chapter for that. Many sources vs sparse). Something like, Figure blah is a residual TS map showing an example of what a typical RoI might look like before

running `addSrcs` and after] [JAM: talk about the prelim SNR cat tests with 6 SNRs here? See what was said about the tests in the SNR cat]

5.3 Galactic Supernova Remnants

[JAM: from SNRcat] In this work we focus on the 279 currently known Galactic SNRs. They are derived from the 274 SNRs noted in the catalog of Green (2009, hereafter Green's catalog), plus five additional SNRs identified following its publication. All but 16 of these SNRs have been identified by their radio synchrotron emission, so their centroids and extensions are primarily determined from the radio. When the radio detection is not securely identified through the synchrotron emission, positional information is obtained from the optical, X-ray, or TeV observations that identified the SNR, as noted in Green's catalog. The catalog is thought to be complete down to a 1 GHz radio surface brightness limit of $\approx 10^{-20}\,\mathrm{W\,m^{-2}\,Hz^{-1}\,sr^{-1}}$ (i.e. $1\,\mathrm{MJy\,sr^{-1}}$). However, selection effects are known to bias radio surveys against the identification of radio faint and small angular size remnants (Brogan et al. 2006; Green 2004). We note that as this work neared completion, a revised catalog of 294 SNRs was published (Green 2014), representing only a small increase ($< 10\%$) over the previous catalog.

5.4 Analysis Methods

[JAM: from SNRcat] To systematically analyze the *Fermi*-LAT γ-ray data, we apply a maximum likelihood (Mattox et al. 1996) framework to RoIs centered on known SNRs (Green 2009). For each SNR, we begin by constructing a model for the spectral and spatial dependence of the γ-ray emission which includes significant point sources in the RoI. We then test for the existence of a γ-ray source near the center. This

includes determining the most likely position and extension of the candidate source and testing for spectral curvature, rather than assuming it follows a PL across the energy range studied. In cases where we find no significant source associated with the SNR, we calculate upper limits on the flux. We calculate both statistical and systematic errors, where the latter are estimated from both the uncertainty in the effective area and the effects of changing the interstellar emission model (IEM), which accounts for γ-rays produced by CR interactions with interstellar gas and radiation fields in the Milky Way.

This analysis uses both the standard Science Tools (version 09-32-05), including `gtlike`, and the `pointlike` analysis package (Kerr 2010) which has been developed and verified for characterizing source extension for *Fermi*-LAT data (Lande et al. 2012). §5.5 describes our data selection; §5.6 details our new method for automatically finding point sources in the *Fermi*-LAT γ -ray emission; and §5.8 discusses the detection method.

5.5 Data Selection

[JAM: from SNRcat] This catalog was constructed using 3 years of LAT survey data from the Pass 7 (P7) "Source" class and the associated P7V6 instrument response functions (IRFs).This interval spans 36 months, from 2008 August 4 to 2011 August 4 (mission elapsed time $239557417 - 334108806$). The Source event class is optimized for the analysis of persistent LAT sources, and balances effective area against suppression of background from residual misclassified charged particles. We selected only events within a maximum zenith angle of 100° and use the recommended fil-

ter string "DATA_QUAL==1 && LAT_CONFIG==1" in `gtmktime`[1]. The P7 data and associated products are comparable to those used in the other γ-ray catalogs employed in this work. We used the first three years of science data for which the associated IEM is suitable for measuring sources with extensions $> 2^{\circ}$[2]. A detailed discussion of the instrument and event classes can be found in Atwood et al. (2009) and at the *Fermi* Science Support Center[1].

For each of the 279 SNRs we modeled emission within a 10° radius of the SNR's center. As a compromise between number of photons collected, spatial resolution, and the impact of the IEM, we chose 1 GeV as our minimum energy threshold. The limited statistics in source class above 100 GeV motivated using this as our upper energy limit.

To avoid times during which transient sources near SNRs were flaring, we removed periods with significant weekly variability detected by the *Fermi* All-sky Variability Analysis (FAVA) (Ackermann et al. 2013). We conservatively defined a radius within which a flaring source may significantly affect the flux of a source at the center. We take this distance to be the radio radius of an SNR plus 2.8°, corresponding to the overall 95% containment radius for the *Fermi*-LAT point spread function (PSF) for a 1 GeV photon at normal incidence (Ackermann et al. 2012c). The time ranges of FAVA flares within this distance were removed in 23 RoIs, leaving $\geq 98.9\%$ of the total data in each RoI.

[1]See LAT data selection recommendations at: `http://fermi.gsfc.nasa.gov/ssc/data/analysis/documentation/Cicerone/Cicerone_Data_Exploration/Data_preparation.html`.

[2]See the LAT caveats, `http://fermi.gsfc.nasa.gov/ssc/data/analysis/LAT_caveats.html`, particularly those for the IEM developed for Pass 7 reprocessed data described in `http://fermi.gsfc.nasa.gov/ssc/data/access/lat/Model_details/FSSC_model_diffus_reprocessed_v12.pdf`.

5.6 Input Source Model Construction

[JAM: from SNRcat] To characterize each candidate SNR we constructed a model of γ-ray emission in the RoI which includes all significant sources of emission as well as the residual background from CRs misclassified as γ-rays. We implemented an analysis method, built upon the `addSrcs` method described in 5.2, to create and optimize the 279 models for each of the 279 RoIs. For each RoI, we initially included all sources within the 10° RoI listed in the Second Fermi LAT source catalog (2FGL) (Nolan et al. 2012), based on 2 years of Source class data. To this we added pulsars from the Second Fermi LAT catalog of Gamma-ray Pulsars (2PC) (Abdo et al. 2013), based on 3 years of source class data, with 2PC taking precedence for sources that exist in both. For the diffuse emission we combined the standard IEM corresponding to our P7 data set, gal_2yearp7v6_v0.fits, with the standard model for isotropic emission, which accounts for extragalactic diffuse γ-ray emission and residual charged particles misclassified as γ-rays. Both the corresponding isotropic model, iso_p7v6source.txt, and the IEM are the same as used for the 2FGL catalog analysis[3].

Compared to 2FGL, we used an additional year of data and limited the energy range to $1 - 100$ GeV. This can result in different detection significances and localizations than previously reported in 2FGL. To account for these effects, we recreated the RoIs' inner 3° radius regions, which encompass the radio extents of all known SNRs, observed to be $\leq 2.6°$ and allows a margin for the LAT PSF. The weighted average 68% containment radius of the LAT PSF for events at 1 GeV is $\sim 0.7°$ (**?**). We note that this implicitly assumes that an SNR's GeV extent should not be more

[3]Further details on the diffuse emission models are available at `http://fermi.gsfc.nasa.gov/ssc/data/access/lat/BackgroundModels.html` [JAM: and in Chapter blah]]

than about an order of magnitude larger than its radio extension and also note that the selection biases stated in Green's catalog limit the range of known SNRs' radio extensions.

To build the inner 3° radius model of each RoI, we first removed all sources except identified active galactic nuclei (AGN) and pulsars, whose positions on the sky are independently confirmed by precise timing measurements (Abdo et al. 2013). Retained AGN were assigned their 2FGL positions and spectral model forms. Pulsars' positions and spectral forms were taken from 2PC. 2FGL sources identified or associated with SNRs are removed when they lie within the inner 3°.

Using `addSrcs`, we generated a TS map via `pointlike` on a square grid with $0.1^\circ \times 0.1^\circ$ spacing that covers the entire RoI. At the position of the maximum TS value, we added a new point source with a Power Law (PL) spectral model:

$$\frac{dN}{dE} = N \frac{(-\Gamma + 1)E^{-\Gamma}}{E_{\rm max}^{-\Gamma+1} - E_{\rm min}^{-\Gamma+1}} \tag{5.4}$$

where N is the integrated photon flux, Γ is the photon index, and $E_{\rm min}$ and $E_{\rm max}$ are the lower and upper limit of the energy range in the fit, set to 1 GeV and 100 GeV, respectively. We then performed a maximum likelihood fit of the RoI to determine N and Γ and localized the newly added source. The significance of a point source with a PL spectral model is determined by the χ^2_n distribution for n additional degrees of freedom for the additional point source, which is typically slightly less than $\sqrt{\rm TS}$

To promote consistent convergence of the likelihood fit, we limited the number of free parameters in the model. For sources remaining after the removal step, described above, we freed the normalization parameters for the sources within 5° of the RoI center, including identified AGN and pulsars. For 2FGL sources between 5° and 10°, we fixed all parameters. The spectrum of the IEM was scaled with a PL whose normalization and index were free, as done in 2FGL. For the isotropic emission

model, we left the normalization fixed to the global fit value since the RoIs are too small to allow fitting the isotropic and Galactic IEM components independently. The isotropic component's contribution to the total flux is small compared to the IEM's at low Galactic latitudes.

After localizing them, the new sources were tested for spectral curvature. In each of the four energy bands between 1 and 100 GeV, centered at 1.8, 5.6, 17.8 and 56.2 GeV, we calculated the TS value for a PL with spectral index fixed to 2 and then summed the TS values. We refer to this as $\mathrm{TS}_{\mathrm{bandfits}}$. A value for $\mathrm{TS}_{\mathrm{bandfits}}$ much greater than the TS calculated with a PL ($\mathrm{TS}_{\mathrm{PL}}$) suggests that, with a more rapid calculation, that the PL model may not accurately describe the source. Analogously to 2FGL, we allow for deviations of source spectra from a PL form by modeling sources with a log-normal model known colloquially as LogParabola or logP:

$$\frac{dN}{dE} = N_0 \left(\frac{E}{E_b}\right)^{-(\alpha+\beta\log(E/E_b))} \tag{5.5}$$

where N_0 is the normalization in units of photons/MeV, α and β define the curved spectrum, and E_b is fixed to 2 GeV[4]. If $\mathrm{TS}_{\mathrm{bandfits}} - \mathrm{TS}_{\mathrm{PL}} \geq 25$, we replaced the PL spectral model with a logP model and refit the RoI, including a new localization step for the source. We retained the logP model for the source if the global log likelihood across the full band improved sufficiently: $\mathrm{TS}_{\mathrm{curve}} \equiv 2(\log\mathcal{L}_{\mathrm{logP}} - \log\mathcal{L}_{\mathrm{PL}}) \geq 16$. Otherwise we returned the source to the PL model which provided the better global log likelihood. Across all RoIs, less than 2% of the newly added sources retained the logP model.

We continued iteratively generating TS maps and adding sources within the entire RoI until additional new sources did not significantly change the global likelihood of the fit. The threshold criterion was defined as obtaining TS < 16 for three

[4]Note: E_b is a scale parameter which should be set near the lower energy range of the spectrum being fit and is usually fixed, see Massaro et al. (2004)

consecutively added new sources, denoted as $N_{TS<16} = 3$. Despite iteratively adding a source at the location of the peak position in the TS map, the TS values of new sources may not decrease monotonically with iteration for several reasons. First, source positions were localized after fitting the RoI and generating the TS map. Second, some added sources were fit with a more complex spectral model than a simple PL. Finally, when creating the TS map, we fixed the source's spectral index to 2, whereas when adding the actual source to the model, we allowed its index to vary.

The specific value of $N_{TS<16} = 3$ was chosen to avoid missing sources with TS ≥ 25 (the threshold commonly used for source detection in LAT data), and to optimize computation time. We tested the threshold by selecting eight representative SNRs from both complex and relatively simple regions of the sky, with both hard and soft spectral indices. The eight chosen regions were:

SNR043.3-00.2 (W49B): A relatively simple region and test case that was previously detected as a point-source SNR (Abdo et al. 2010b)

SNR034.7-00.4 (W44): Previous LAT studies showed the SNR had a GeV extension slightly larger than the radio size as well as surrounding GeV emission from nearby extended sources associated with molecular clouds (Abdo et al. 2010c; Uchiyama et al. 2012)

SNR078.2+02.1 (gamma Cygni): A complex region containing the SNR an embedded pulsar, several nearby pulsars, and a large diffuse structure known as the Cygnus cocoon which is believed to be a bubble of hot gas acting as a source of freshly accelerated CRs (Ackermann et al. 2011, 2012b). The region serves as a test of how robust `addSrcs` is in one of the more extreme RoIs. Despite the complexity of the region, Lande et al. (2012) detected GeV emission co-spatial with the radio SNR.

SNR027.4+00.0 (Kes 73), SNR031.9+00.0 (3C391), SNR292.2-00.5, SNR332.4-00.4 (MSH 16-51), SNR205.5+00.5 (Monoceros): These five sources were found to have large fitted extensions (greater than twice the radio radius of the SNR) in preliminary SNRcat pipeline runs so were included to understand this occurrence.

We applied the procedure detailed above to the test RoIs using a criterion of $N_{TS<16} = 6$ and counted how many $TS \geq 25$ sources would be excluded if a smaller $N_{TS<16}$ criterion was used. Figure 5.2 shows how reducing the threshold to $N_{TS<16} = 3$ cut only one significant source in any of the regions. A further criteria to validate the value of $N_{TS<16}$ used in this paper was that the spectrum of a source of interest (i.e. the central extended SNR in an RoI) or extension was robust to the addition of nearby sources. In Figures 5.3, 5.4, and 5.5, we show an example of the evolution of the flux, index, and extension of SNR gamma Cygni as subsequent sources are added. Sources were added to the ROI until $\Delta(\log \mathcal{L}) < 8$, 6 times in a row, and see that while a significant source added close to the SNR can affect the fit of the extended source, these fits stabilize before our threshold is reached. Since the maximum number of sources added in any test RoI was 38, the minimum 14, and the total number of sources added across all test regions was 221, we chose to use $N_{TS<16} = 3$ for the full sample of 279 RoIs.

To allow for proper convergence of the likelihood fit, we reduced the number of free parameters prior to each new source addition. If the previously added source was between 3° and 5° of the center of the RoI, just its normalization was freed, and if greater than 5° all its source parameters were fixed. To avoid having newly added sources overlap with pulsars, we deleted new sources from the RoI if they were within 0.2° of a γ -ray pulsar and refit the pulsar in the $1 - 100$ GeV range following the 2PC conventions. 2PC modeled pulsar spectra as a PL with an exponential

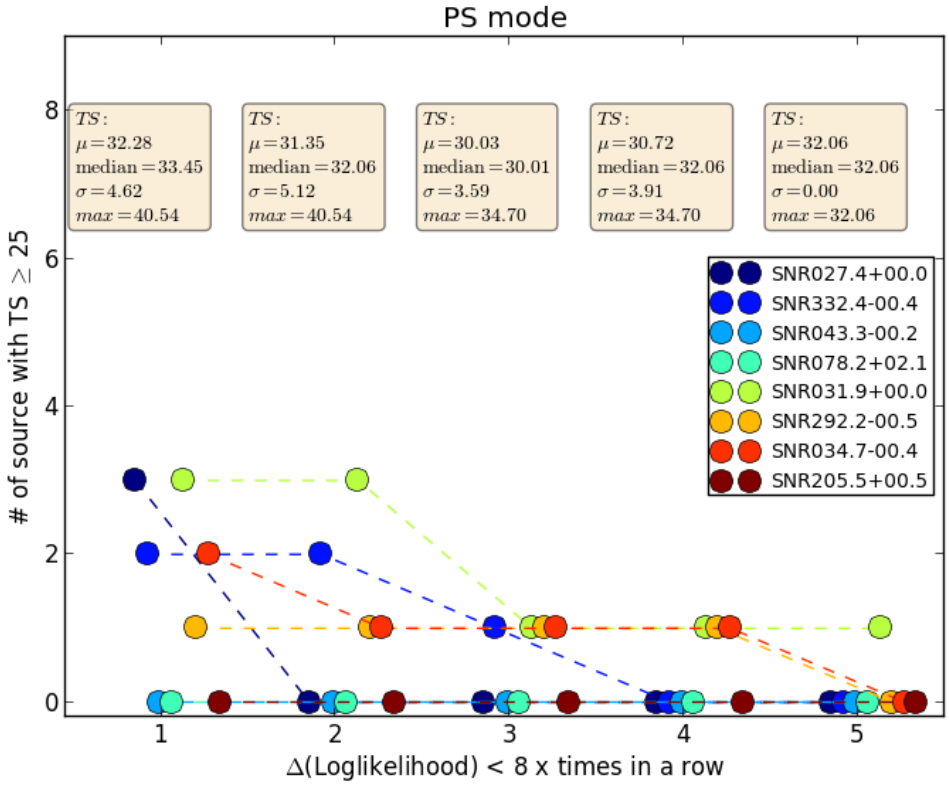

Figure 5.2: Histogram of the number TS $\geq$ 25 sources remaining in each of the 8 test RoI for iterations in which $\Delta(\log \mathcal{L}) < 8$ (i.e. TS < 16). Points are offset for each SNR for clarity. The text boxes detail statistics for the values of TS of significant sources for the 8 studied SNRs for each corresponding value on the x-axis.

cutoff (PLEC),

$$\frac{dN}{dE} = N_0 \left(\frac{E}{E_0}\right)^{-\Gamma} \exp\left(-\frac{E}{E_c}\right)^{b}, \tag{5.6}$$

where N_0 is the normalization factor, Γ is the photon spectral index, E_c the cutoff energy, and b determines to the sharpness of the cutoff. 2PC assessed the validity of fixing b to 1 in Equation 5.6 (PLEC1) by repeating the analysis using a PL model, as well as the more general exponentially cut off PL form, allowing the parameter b in Equation 5.6 to vary. For the pulsar spectra in this analysis, we compared the maximum likelihood values for spectral models with and without a cutoff and with and without the value of b being free, via $\mathrm{TS}_{\mathrm{cut}} \equiv 2(\log \mathcal{L}_{\mathrm{PLEC1}} - \log \mathcal{L}_{\mathrm{PL}})$ and

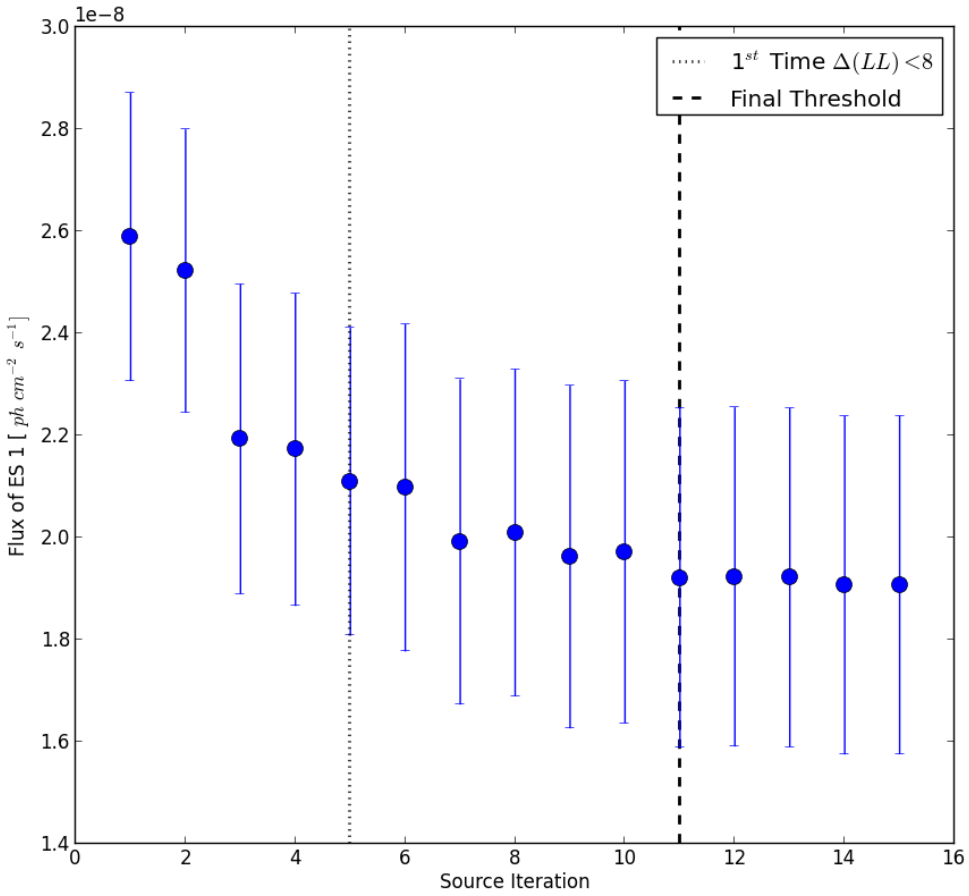

Figure 5.3: Flux evolution of the extended source coincident with SNR gamma Cygni (labeled ES 1 in the figure) as successive sources are added to the ROI. Dotted line is first time $\Delta(\log \mathcal{L}) < 8$, dashed line shows the final threshold for this test study.

$\mathrm{TS}_b \equiv 2(\log \mathcal{L}_{\mathrm{PLEC}} - \log \mathcal{L}_{\mathrm{PLEC1}})$ to determine which to use. If $\mathrm{TS}_{\mathrm{cut}} < 9$ is reported for the pulsar in 2PC then a PL model is used. If $\mathrm{TS}_{cut} \geq 9$, we then check to see if the cutoff energy fit in 2PC lies within the restricted energy range of $1 - 100\,\mathrm{GeV}$ used in this work. For pulsars with cutoffs $\geq 1\,\mathrm{GeV}$, we then use the PLEC model if $\mathrm{TS}_{\mathrm{b}} \geq 9$, and the PLEC model with cutoff freed otherwise. For those pulsars with cutoffs less than 1 GeV the spectral parameters are fixed to the 2PC values.

To complete the construction of our point source RoI model, we took the output

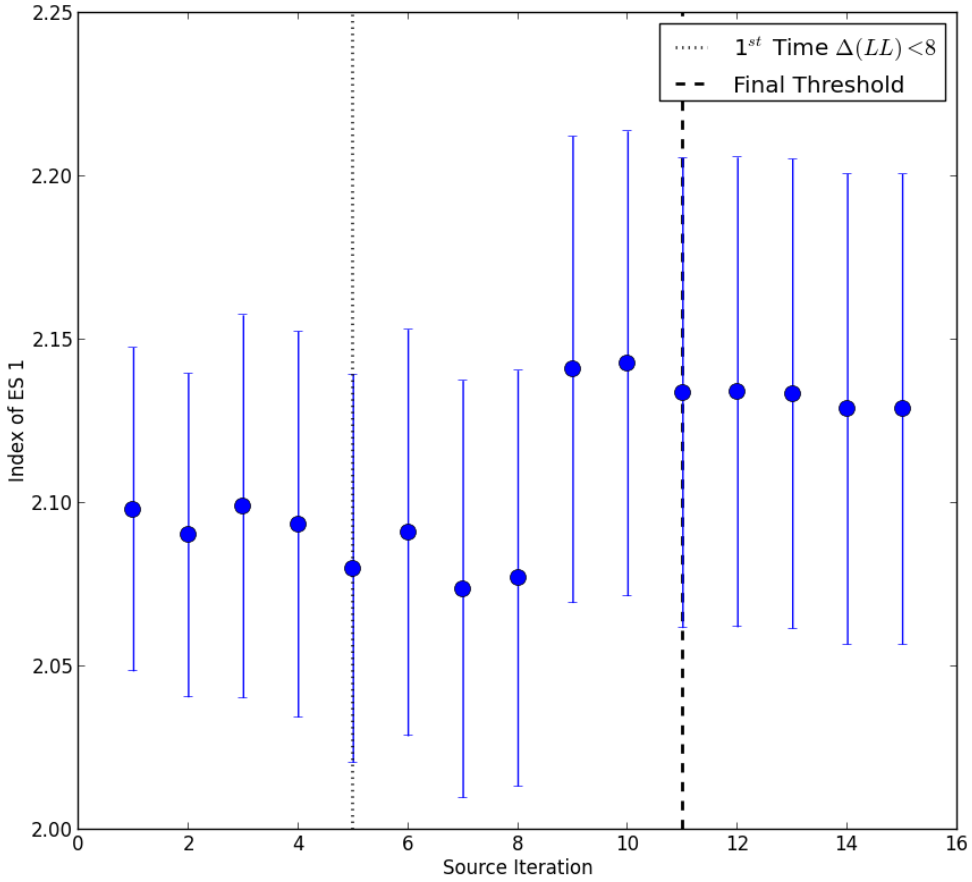

Figure 5.4: Same as Figure 5.3 but for the PL spectral index.

of the previous steps and removed all sources with TS < 16. This final model was then used as the starting model for analyzing candidate SNR emission. In Figure 5.6, we show a residual TS map of the region around SNR W44 as an example of the source configuration in an RoI prior to running `addSrcs`. Figure 5.7 is a residual TS map of the same region after running `addSrcs` to decompose the region into point sources.

We conservatively allow sources with TS down to 16 ($\sim 4\,\sigma$) in order to account for the effects of at least the brightest sub-threshold sources on the parameter fits for the other sources in the model. Furthermore, while the SNR analysis method

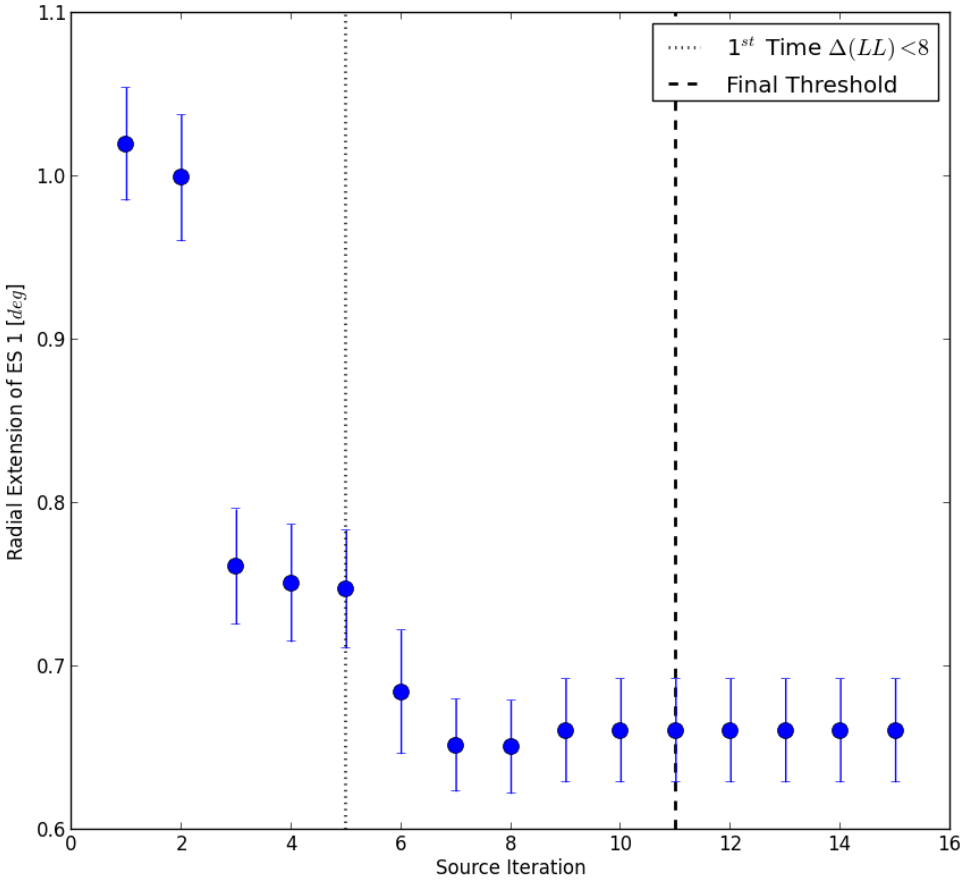

Figure 5.5: Same as Figure 5.3 but for the radius of a uniform, symmetric disk.

described in the chapter 5.8 is allowed to remove sources, it cannot add them. Thus we start from a set of sources designed to allow the final model to capture all significant emission within the central region. To corroborate our method of systematically adding sources to a region, we compare our RoI source models with those found by the 2FGL approach in Chapter 5.7.

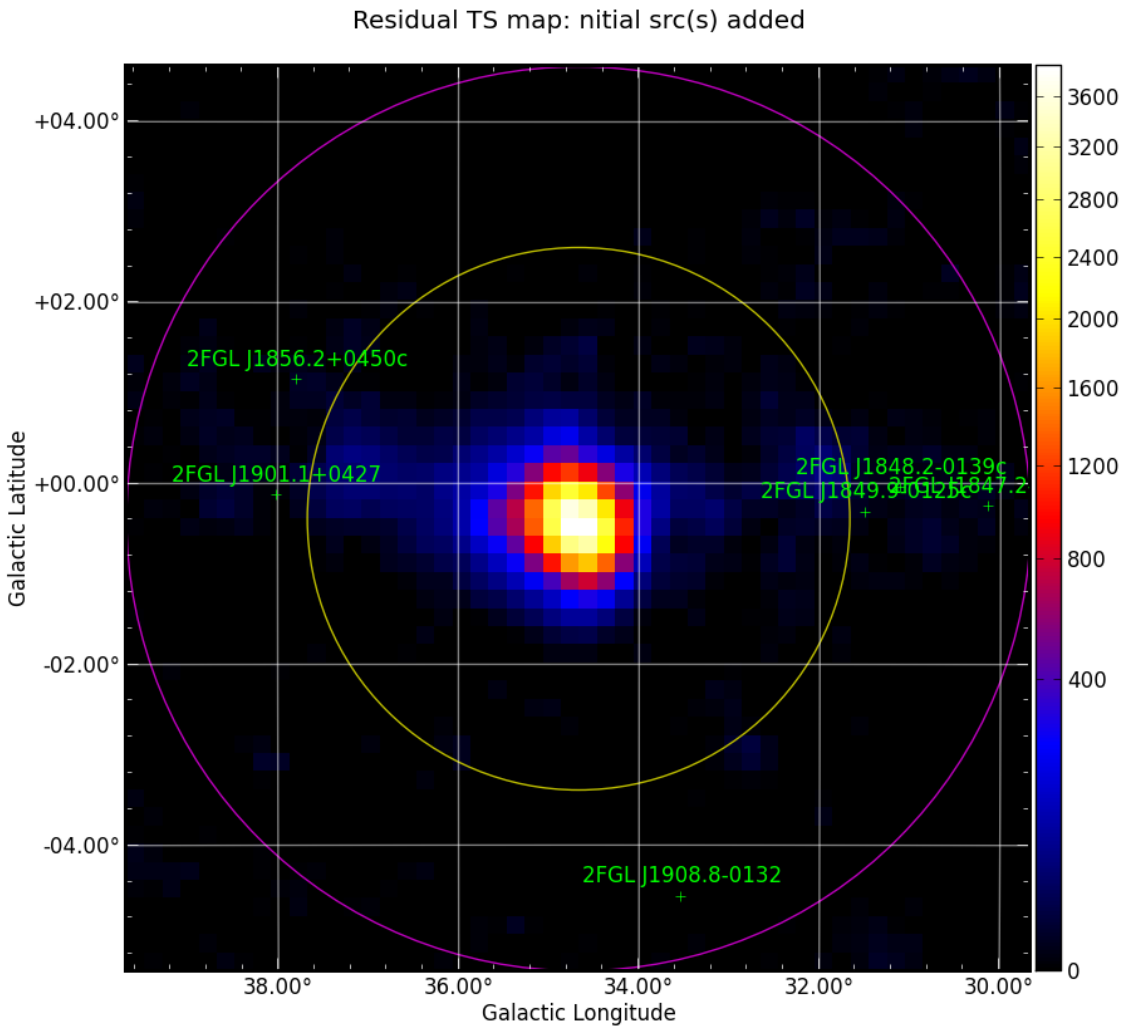

Figure 5.6: 1-100GeV residual TS map for SNRW44 before running `addSrcs` and with 2FGL sources removed from the inner 3° radius (yellow circle). Bin size is 0.2/pixel. Magenta circle shows a 5° radius. 2FGL and newly added sources are shown as green crosses.

5.7 Comparison of Source Models with 2FGL

[JAM: from SNRcat]This SNR catalog was constructed using 3 years of P7 Source class data in the energy range $1-100$ GeV, whereas 2FGL used 2 years of data over the larger energy range $0.1-100$ GeV. The differences in observing time and energy range resulted in residual, unmodeled emission in some RoIs as well as changes to some 2FGL sources' spectral model, position localization, and detection significance.

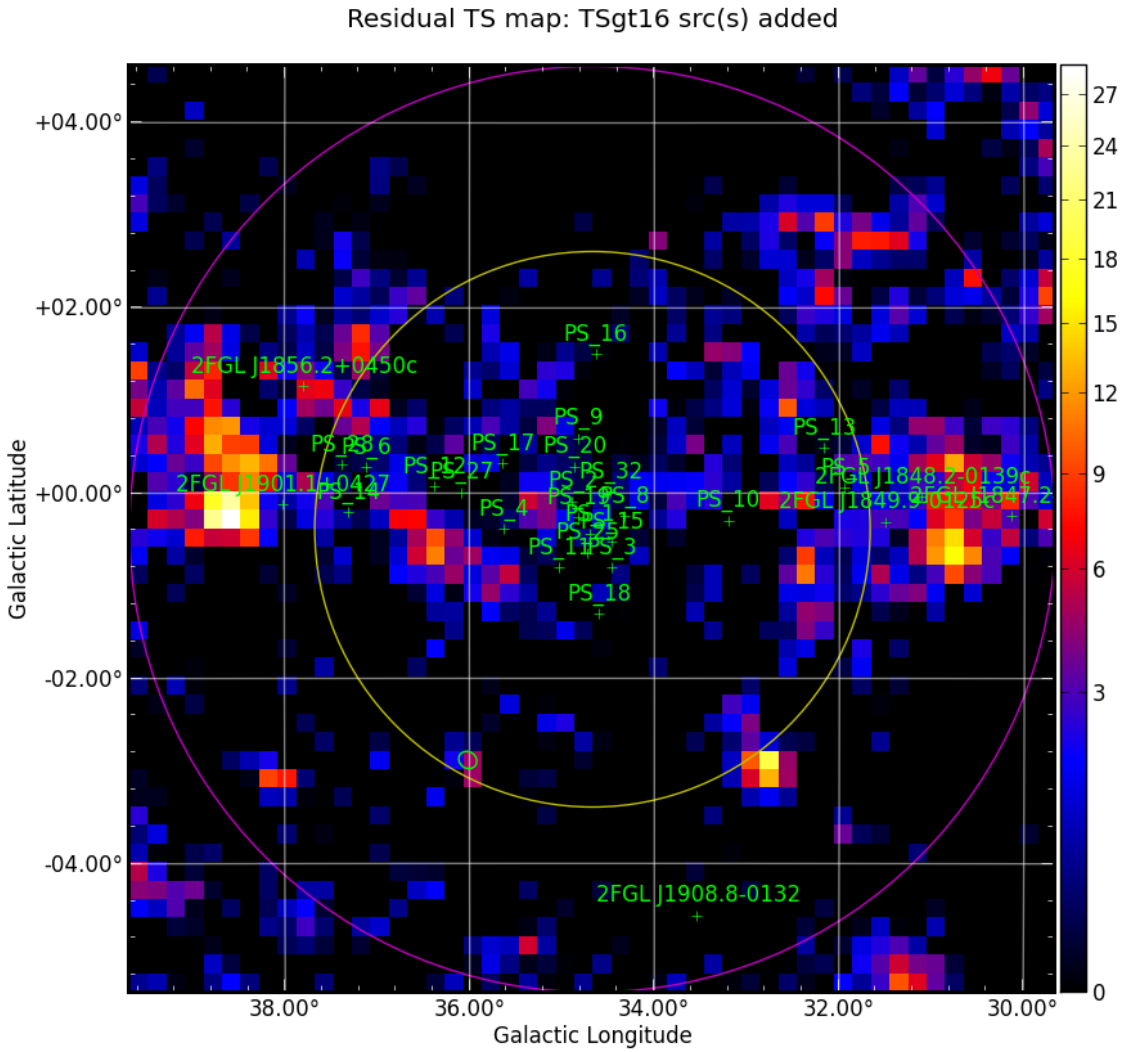

Figure 5.7: 1-100GeV residual TS map for SNR W44 after `addSrcs` has completed. 2FGL sources have been removed from the inner 3° radius (yellow circle), and the bin size is 0.2/pixel. Magenta circle shows a 5° radius. 2FGL sources are shown as green crosses.

Here we compare the input source models constructed for this catalog, described in Chapter 5.6, with 2FGL to better understand the `addSrcs` method's ability to describe the regions studied. Since we rederive the input source model only within a 3° radius of the center of each RoI, we consider sources only inside that radius.

Given the data set differences, in each RoI we expect similar but not identical numbers of sources relative to those in 2FGL. Figures 5.8 and 5.9 show the numbers

of significant ($TS \geq 25$) 2FGL sources and derived input model sources (excluding 2FGL identified AGN and pulsars kept in the input model) in individual RoIs as 2D histograms. In Figure 5.8, the number of sources in the derived input model is typically greater than the number of 2FGL sources that are significant at $1 - 100\,\mathrm{GeV}$. 73 of the 279 RoIs studied contain at least one of the the 12 extended 2FGL sources. Since 2FGL extended sources were removed from the inner 3° of each RoI, and this region was repopulated with point sources, we can detect multiple point sources inside the extent of any removed extended 2FGL sources. This decomposition of extended sources, combined with the longer data set and different energy range compared to 2FGL, contribute to the high ratio of input model to 2FGL sources in some RoI, which demonstrates the need to rederive the source model.

To more accurately represent the 2FGL sources being reproduced in the central 3°, in Figure 5.9 we limited the input model sources to those within 0.2° (approximately the width of the core of the 10 GeV PSF) of a 2FGL source, effectively excluding input sources that are not co-spatial with a 2FGL source. Here we see that the majority of 2FGL sources have counterparts in the rederived set. As a region's complexity increases, seen as an increase in numbers of 2FGL sources, up to about half of the 2FGL sources may not have counterparts within 0.2°. Given that in these same regions we have more new sources than 2FGL sources, as seen in Figure 5.8, we find as expected that the longer data set with improved statistics at higher energies, where the angular resolution of the LAT is the best, allows us to add new sources to account for newly significant excesses in these complex regions. Additionally, sources with low TS in 2FGL are particularly susceptible to having a newly added source which may start at a similar position but then localize further than 0.2° from the 2FGL source.

Thus, we find that the method developed and used here produces a model which

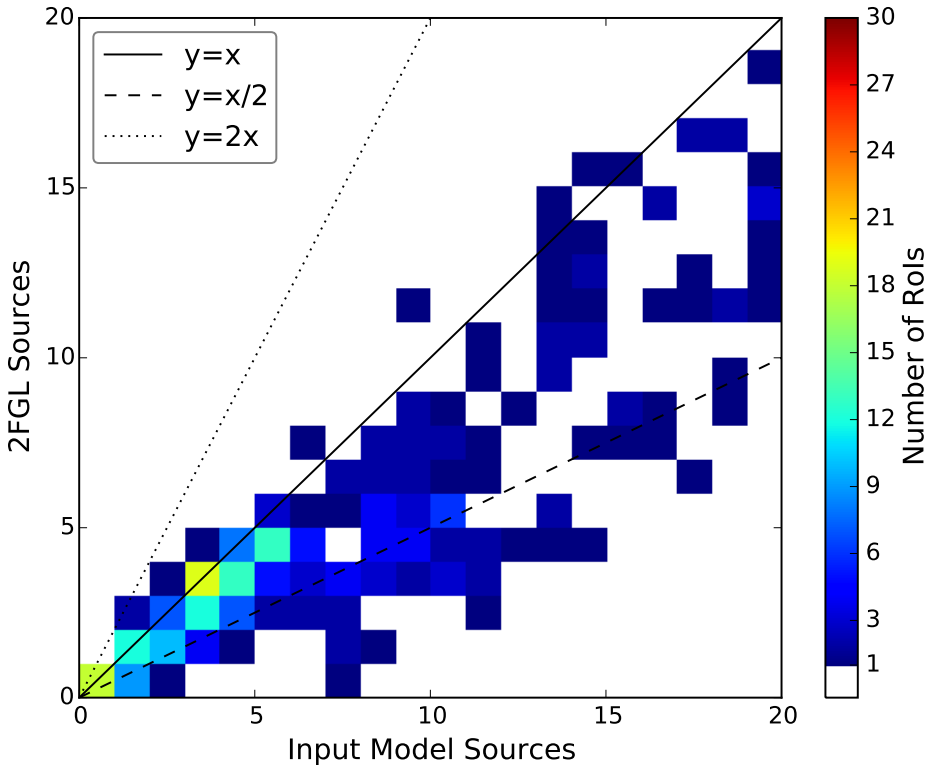

Figure 5.8: Comparison of the number of 2FGL sources with $TS_{1-100\,GeV} \geq 25$ (excluding AGN and pulsars) with the number of newly added input model sources in the present analysis, for sources within 3° of the center of each RoI. The color scale shows the number of RoIs with a particular combination of numbers of 2FGL sources and new sources. White corresponds to no RoI with that combination of source counts.

reproduces the 2FGL sources as expected, including differences that trend as anticipated given the longer data set and modified energy range, yielding better spatial resolution. The new method thus provides reasonable representations of the regions being modeled as input for the final analysis.

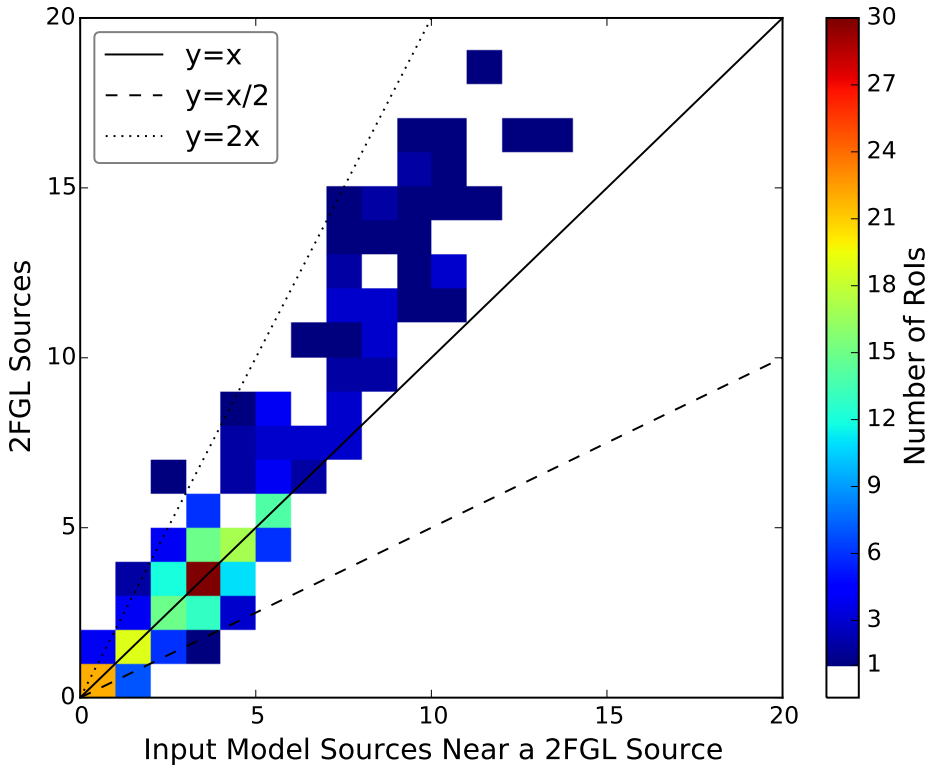

Figure 5.9: Same as Figure 5.8, including only input model sources lying within 0.2° of a 2FGL source.

5.8 Detection Method

[JAM: from SNRcat]For each SNR, we characterize the morphology and spectrum of any γ-ray emission that may be coincident with the radio position reported in Green's catalog. This was achieved by testing multiple hypotheses for the spatial distribution of γ-ray emission: a point source and two different algorithms for an extended disk. The best fit was selected based on the global likelihoods of the fitted hypotheses and their numbers of degrees of freedom. The hypothesis with the best global likelihood was then evaluated using a classification algorithm described in Acero et al. (2016) to determine whether the radio SNR could be associated with the detected γ-ray emission.

Spatial coincidence is a necessary but not sufficient criterion to identify a γ-ray source with a known SNR. The detection of spatially extended γ-ray emission increases confidence in an identification, especially if GeV and radio sizes are similar, as has been observed on an individual basis for several extended SNRs (e.g. Lande et al. 2012). The LAT has sufficient spatial resolution to detect many Galactic SNRs as extended. Figure 5.10 shows the distribution of radio diameters from Green's catalog. Vertical dashed lines show the minimum detectable extension for sources with flux and index typical of those observed in this catalog, based on simulations using the P7V6 IRFs (Lande et al. 2012). The minimum detectable extension depends not only on the source's flux and spectrum, but also the flux of the background, which was estimated by scaling the average isotropic background level by factors of 10 and 100 to be comparable to the Galactic plane. As figure 5.10 illustrates, roughly one third of the known Galactic SNRs may be resolved by the LAT if they are sufficiently bright GeV sources.

In order to determine the best representation for each SNR, we analyzed each SNR-centered RoI using multiple hypotheses for the spatial and spectral form. We used `pointlike` (Kerr 2010) to compare PL and logP spectral forms, to compare point source versus extended source hypotheses, and to analyze the robustness of sources near the extended source.

For each hypothesis, we started with the input model described in Chapters 5.5 and 5.6. We removed sources falling within the SNR's radio disk unless they had been identified as an AGN or pulsar, as described in Chapter 5.6. We then proceeded to evaluate the following point and extended source hypotheses. For the point source hypothesis, a point source with a PL index initialized to 2.5 was placed at the radio centroid of the SNR. The positions, spectral index, and spectral normalization of the point source were then fit. As for the initial input model described in Chapter 5.6,

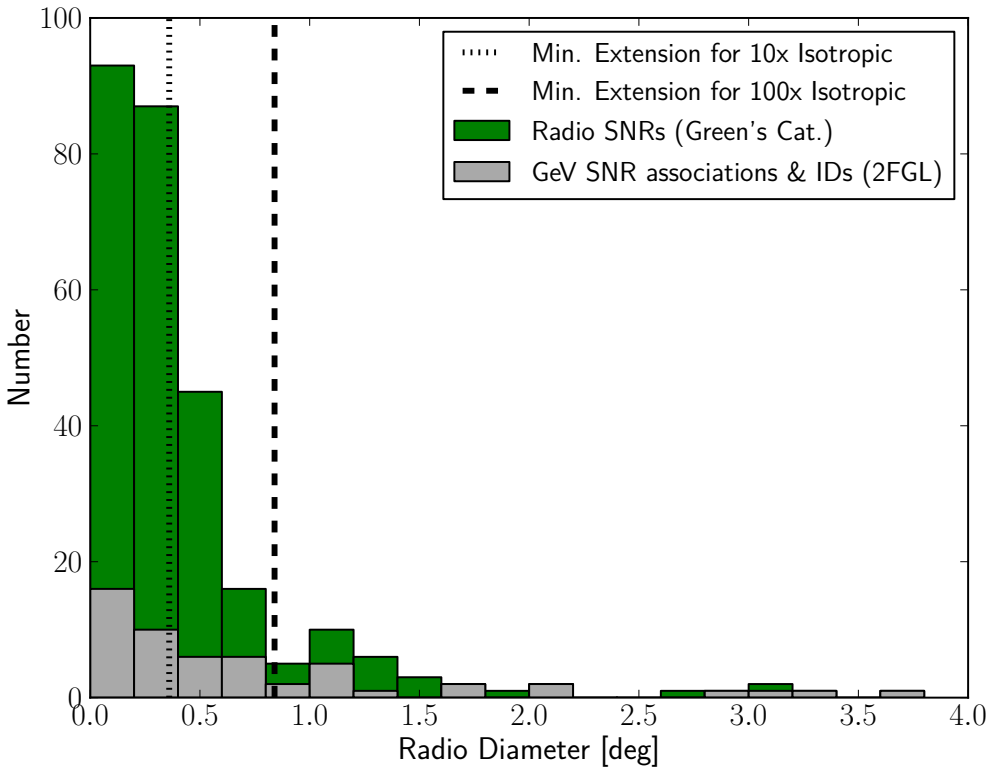

Figure 5.10: Distribution of SNR radio diameters from Green's catalog. The vertical dashed lines indicate the minimum detectable extension for a source with a photon flux of $10^{-8}\,\mathrm{ph\,cm^{-2}\,s^{-1}}$ in the $1-100\,\mathrm{GeV}$ energy range and a PL index of -2.5, from simulations of 2 years of data and the P7V6 IRFs (Lande et al. 2012). In that work, simulations using 10x and 100x the isotropic background level (thin-dotted and thick-dashed lines) are used to estimate a reasonable background range for sources in the Galactic plane.[JAM: idk what plots are ok or not to include from papers I am an author on. I didnt make this plot, but I made the first version of it that inspired this one. Should I specifically include a comment for these plots that state they're from the snr cat vs ones not in the paper?]

we tested the source for spectral curvature. To test the extended source hypothesis, we employed two separate procedures. Both employed a uniform disk model initially placed at the center of the RoI with a radius equal to that observed in the radio. In the first procedure, called the "disk" hypothesis, we fit both the position and extension of the disk, as well as tested for spectral curvature. A second procedure, which results in a model we call the "neardisk" hypothesis, additionally examines

the significance of sources nearby the disk, removing those which are not considered independently significant and refitting the disk position and radius. This procedure is described in Chapter 5.8.1.

Having evaluated these hypotheses, we compared the global likelihood values of the final extended hypothesis and of the point source hypothesis to determine which model had the largest maximum likelihood. If the source is significant in the best hypothesis, the model parameters are reported as Tables 1 and 2 in Acero et al. (2016) [JAM: should I include abridged tables?]. If no hypothesis had a significant γ-ray source coincident with the radio SNR, we calculated the upper limit on the flux from a region consistent with the radio SNR, described in Chapter 5.8.2, and report the results in Table 3 in Acero et al. (2016). [JAM: should I include the tables here? only if they're short, or abridged. I should def include the dist table because I did that work]

5.8.1 Localization, Extension, and Spectral Curvature

[JAM: from SNRcat]To test our hypotheses, we combined the initial model of point sources (Chapter 5.6) and the Galactic and isotropic diffuse contributions (Chapter 5.5 and 5.6) with a test source at the center of each RoI. All sources that fell within the radio SNR radius other than previously identified AGN or pulsars were removed, as was done for the input source model (Chapter 5.6). We note that multiple point sources removed within a single radio SNR radius may represent substructure within the source itself. This process conservatively assigns the majority of the flux to a single source, rather than decomposing it. We optimized the position of the test source with `pointlike`, iteratively allowing other model parameters to vary. For all hypotheses, the normalizations of all sources within 5° of the radio SNR center were fit while all other spectral parameters were fixed. The parameters for sources

outside 5° were also fixed.

For the point source hypothesis, a point source was placed at the radio centroid of the SNR. For the disk hypothesis, a uniform disk with radius equal to the radio radius was placed at the center. In both hypotheses, the normalization, index, and position of the candidate source were fit. For the disk hypothesis, the extension was also fit. Previous analyses of a range of possible Galactic SNR sources with similar data sets (e.g. Lande et al. 2012) typically showed no differences in global likelihood significant enough to justify choosing a Gaussian over a uniform disk template or vice versa. In addition, there was typically little difference in spectral parameters for the two spatial forms. For simplicity and clarity, we thus test only the uniform disk hypothesis. We allowed the localization to wander up to 5° in the fits as a reasonable upper limit on what might later be associated with the SNR. This is roughly twice the radius of largest radio SNR.

We included an additional disk hypothesis in which we recalculated the significance of each nearby point source. Because neighboring sources can influence the best fit disk parameters, we iteratively evaluated the significance of the neighboring source by calculating $\mathrm{TS}_{\mathrm{nearby}}$, defined as twice the difference between the model's log-likelihood ($\log \mathcal{L}$) with the nearby point source and the model without the source, as determined by `pointlike`. Starting from the fitted disk model, for each neighboring point source we refit the position, extension, normalization, and spectrum of the uniform disk after removing the source. A nearby source was considered to be significant and thus kept if $\mathrm{TS}_{\mathrm{nearby}} \geq 9$. Each point source was evaluated individually, starting with the closest point source and extending radially outward to all sources within 1° of the furthest edge of the SNR's radio disk. The final result of this iterative process is called the "neardisk" hypothesis which, for cases where neighboring source(s) were removed, can have different best fit disk parameters. As

a final step we refit the region with `gtlike`, using the neardisk model.

We chose the best extended source hypothesis by comparing the final disk and neardisk `gtlike` $\log \mathcal{L}$ values. Since the neardisk hypothesis can have fewer degrees of freedom, we chose the final disk hypothesis only if $2\times(\log \mathcal{L}_{\rm disk} - \log \mathcal{L}_{\rm neardisk}) \geq 9$. Otherwise, we used the neardisk model as the final extended source hypothesis, hereafter referred to as the "disk hypothesis".

In some cases a point source could not be localized starting at the SNR center. If the `pointlike` localization failed to converge when starting at the SNR center, we placed the candidate at the position of the most significant source removed from within the radio SNR radius and followed the procedure outlined above. For 69 RoIs there was either no source removed within the radio SNR or localization failed. For 31 RoIs, the candidate found had a TS < 1 and was removed from the model so as not to cause instabilities in the minimization. If the disk hypotheses converged and the final candidate was significant (TS ≥ 25) in both the localization and spectral fits, the best extended hypothesis was selected.

Prior to the final fit of the region, sources were tested for spectral curvature using $\mathrm{TS}_{\rm bandfits} - \mathrm{TS}_{\rm PL} \geq 25$. If this criterion was satisfied then we replaced the PL spectral model with a logP model and refit the RoI. The final spectral model was selected, as for the input model, by comparing the $\log \mathcal{L}$ values, in this case $\mathrm{TS}_{\rm curve} \geq 16$, as defined in Chapter 5.6. Seven sources were found to be significantly better fit by a logP spectrum. To obtain final spectral parameters, we performed a final fit using the standard likelihood analysis tool `gtlike`. The normalization and index parameters were constrained to lie within a physically reasonable range.

We determined the final RoI model by selecting the most likely hypothesis based on a comparison of the `gtlike` global $\log \mathcal{L}$ of the point source hypothesis with the most likely extended source hypothesis. An extended hypothesis was considered

significantly more likely if TS_{ext} was ≥ 16, where TS_{ext} is defined as twice the difference between the $\log \mathcal{L}$ of the final model from the disk hypothesis and that of the point source hypothesis, $TS_{ext} = 2(\log \mathcal{L}_{disk} - \log \mathcal{L}_{point})$, as in Lande et al. (2012). Otherwise, if the point source itself had $TS > 25$, we chose the point source hypothesis. In cases in which the optimization for the position of the point source did not converge but an extended disk was detected, we calculated the global $\log \mathcal{L}$ of the region without any source and with a point source at the center of the extended source. We then use the latter value to calculate TS_{ext} reported in Table 1 in Acero et al. (2016). For these candidates, if the source was significantly extended in both cases, we select the extended hypothesis. If none of the criteria were met, the candidate was considered undetected and we calculated an upper limit on the flux. Both the upper limits and flux calculation are described in the following subsection.

5.8.2 Fluxes and Upper Limits

[JAM: from SNRcat]Fluxes in the $1 - 100\,\mathrm{GeV}$ band are determined using the standard analysis tool `gtlike` by a final fit of the model chosen to have the overall maximum likelihood characterization of the morphology and spectrum of the candidate source from the analysis detailed in Chapter 5.8 and 5.8.1. For those RoIs where no significant source was detected, we computed Bayesian upper limits on the flux using the method in described in Helene (1983) excluding any overlapping sources in the model that have not been identified as AGN or pulsars, as described in Chapter 5.6. As a spatial model we used a uniform disk equal in position and radius to that reported in Green's catalog. We assumed the spectral model to be a PL and report upper limits for indices of 2.0 and 2.5 at 95% and 99% confidence levels. The choice of indices was motivated by the distribution of PL indices for classified sources. The results are reported in Acero et al. (2016).

5.9 Catalog Results

[JAM: from SNRcat] We detected 102 candidates with a final source TS $\geq$ 25 in the 279 SNR RoIs (see Chapter 5.8). Of the 102 detected candidates, 36 passed the association probability threshold (see Acero et al. (2016)). Of these, 30 SNRs ($\sim$ 11% of the total) show significant emission for all alternative IEMs and are classified as likely GeV SNRs. An additional four were identified as sources which are not SNRs.Two other candidates were demoted to marginal due to their dependence on the IEM, as described in the next paragraph. Of the sources likely to be GeV SNRs, 17 show evidence for extension ($TS_{ext} > 16$). Only sources associated with SNRs G34.7−0.4 and G189.1+3.0 show evidence of significant spectral curvature in the $1 - 100$ GeV range and are fit with logP spectra. Of the classified candidates, four extended and 10 point SNRs are new and published here for the first time. Descriptions of the new extended (G24.7+0.6, G205.5+0.5, G296.5+10.0, and G326.3−1.8) SNRs is given in Acero et al. (2016).

For those 245 SNRs that are either not detected by this analysis or which fail to meet the most stringent threshold for classification as a detected SNR, upper limits assuming the radio disk morphology of Green's catalog with PL indices of 2.0 and 2.5 are reported in Table 3 in Acero et al. (2016). For those candidates which fail to meet the most stringent threshold, we replaced the source with the radio disk. We do not calculate upper limits for the four sources which are identified as not SNRs. A FITS version of the catalog is available through the *Fermi* Science Support Center, as described in Acero et al. (2016)[5]. [JAM: not including the detailed description of the new SNRs]

[JAM: all the multiwavelength CR stuff and I wasn't so involved in, but it's kind

[5] `http://fermi.gsfc.nasa.gov/ssc/data/access/lat/1st_SNR_catalog/`

of the crux of the paper. I don't know how much of if it, if any to include here.]

5.10 GeV SNRs in a Multiwavelength Context: Discussion Summary

Here, we summarize some of the findings detailed in the SNRcat that are most pertinent to the work performed for this thesis. [JAM: do I need a statement like this?]

As discussed in Chapter 3.2, the same population of radio, synchrotron-emitting CR electrons active in the shell of an SNR are expected to also produced γ-rays through the IC process and non-thermal bremsstrahlung radiation. If indeed the GeV and radio emission are produced in a single zone, it is reasonable to assume that the radio and γ-ray morphologies will correlate. We find that the best GeV diameter is within errors of the radio diameter for most of the candidates classified as being associated with an SNR, as shown in Figure 5.11. The same, co-spatial, electron population producing the GeV and radio emission is also suggestive of a potential correlation between the radio and γ-ray flux. Figure 5.12 shows the 1 GHz synchrotron flux versus the 1 GeV γ-ray flux for all SNRs. Despite suggestions of correlation, Kendalls τ rank correlation tests suggested no significant correlation exists between the radio and GeV flux or luminosities (not shown here). Various factors, such as the lack of detailed nonthermal emission modeling, distance measurement errors, and use of oversimplified γ-ray spectral models can skew these results, obscuring any inherent correlation.

We test for one further relationship between the radio and GeV emission and the underlying particle populations through the measured radio and GeV spectral indices. The energy of synchrotron-emitting leptons traced by 1 GHz observations

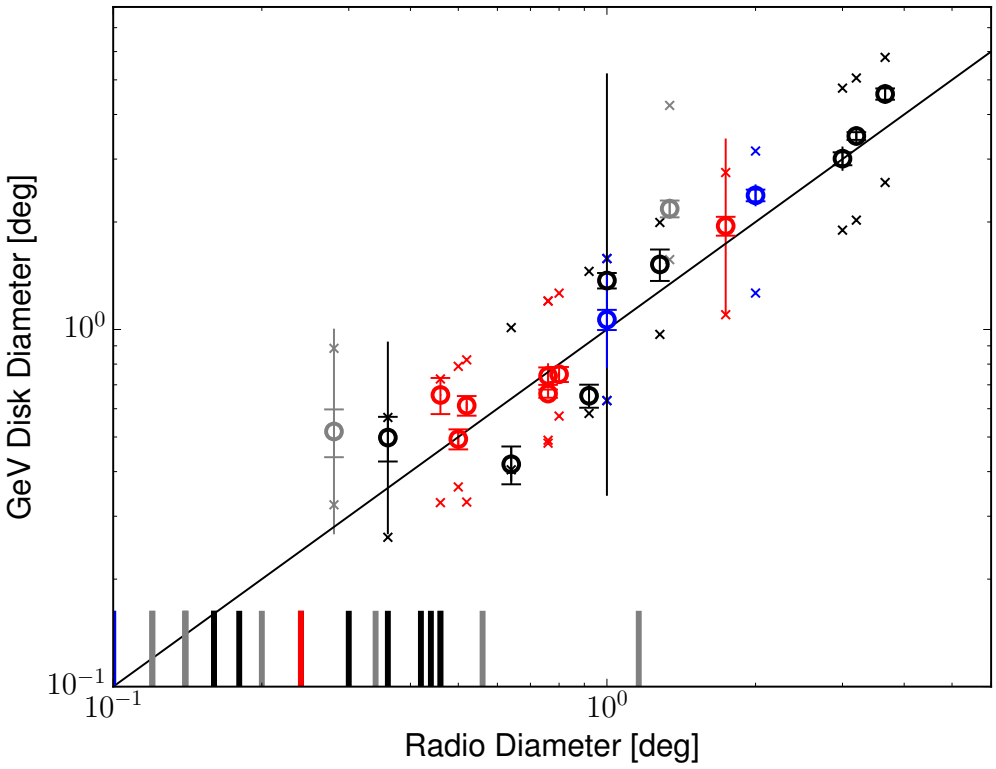

Figure 5.11: Radio diameters of Green's catalog SNRs plotted against the fitted GeV diameters for those candidates with significant extension. The solid line represents equal radio and GeV diameters. All cases of detected extension have diameters greater than 0.2°. The ticks denote the radio extension of GeV point-like candidates, colored in order of their characteristics (young or interacting) and by their classifications (well defined or marginal). The small 'x's bracketing the points show the minimum and maximum GeV extensions allowed such that the source remains classified or marginally classified given the radio position and extension and best fit GeV position. Open circles indicate extended SNRs. All SNRs that passed classification are shown as black unless also classified as young, nonthermal X-ray SNRs (blue) or as interacting with MCs (red). Candidates that did not pass classification but that still had both fractional overlaps > 0.1 are gray. Statistical error bars have caps; error bars without caps represent the systematic error. [JAM: took out the filled circles and outlined part, If they are also young or interacting, they are outlined in blue or red, respectively (No extended marginally classified candidates were also identified as young or interacting.)]

depends on the magnetic field. If radio and GeV emission trace the same underlying particle population, then, at energies below the maximum energy reached by

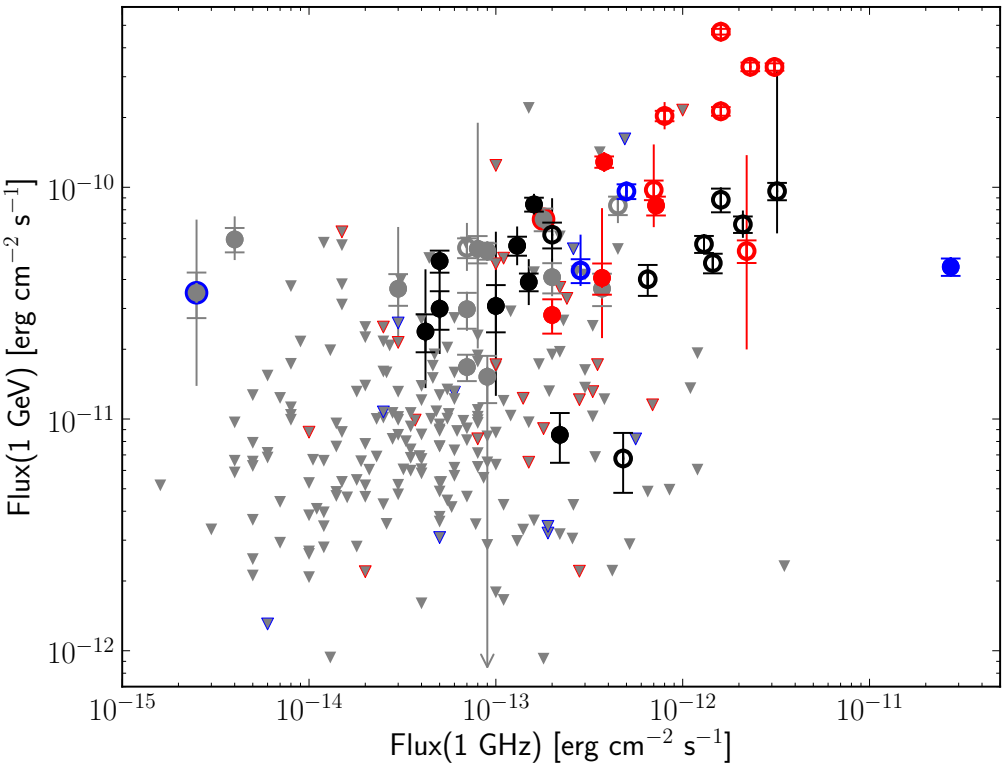

Figure 5.12: Comparison of γ-ray and radio spectral flux densities for all SNRs and candidates. For all SNRs that were not detected or which failed classification, grey triangles indicate upper limits at 99% confidence, computed assuming the radio location and extension. Symbols, colors, and error bars are as in Figure 5.11. In addition, filled circles indicate point-like sources, and if grey markers are also young or interacting, they are outlined in blue or red, respectively (No extended marginally classified candidates were also identified as young or interacting).

the accelerated particles, the photon indices of radio and γ-ray emission should be correlated. For π^0 decay and $e^{\pm}$ bremsstrahlung, the GeV and radio photon indices (Γ and α respectively) are related as $\Gamma = 2\alpha + 1$. For IC scattering leptons, the GeV and radio photon indices follow $\Gamma = \alpha + 1$, or in the case in which high-energy leptons have been cooled via synchrotron or IC radiation, $\Gamma = \alpha + 3/2$ (Reynolds 2008). Figure 5.13 compares the deduced radio spectral index α with the $1-100$ GeV photon index Γ.

Nearly all candidates have γ-ray photon indices that are softer than predicted

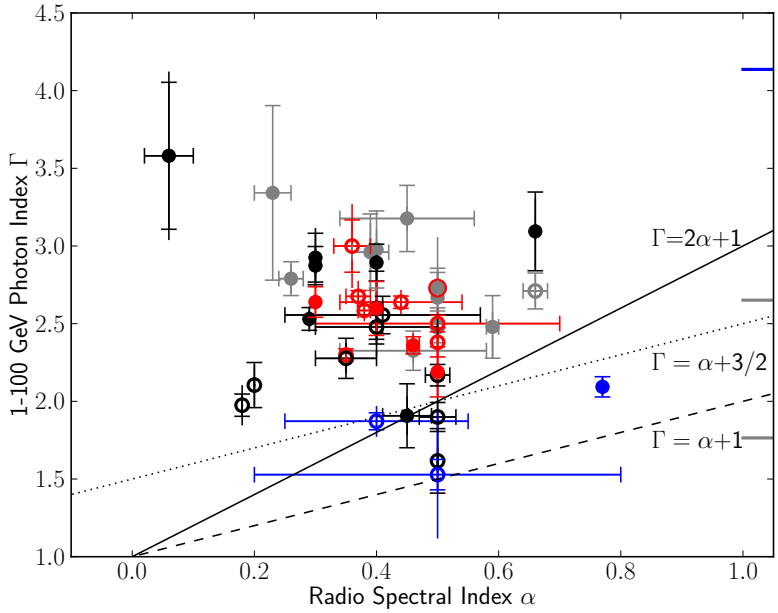

Figure 5.13: Comparison of radio spectral index, α, and GeV photon index, Γ. The expected correlations are plotted for π^0 decay or $e^{\pm}$ bremsstrahlung (solid) and IC emission from an electron population that is freshly accelerated (dashed) or cooled by radiative processes (dotted). Emission via a combination of processes would fall between the lines (e.g. between the solid and dashed for a combination of π^0 decay and IC emission). Symbols, colors, and error bars are as in Figure 5.11; ticks along the right hand side show the $1-100$ GeV photon indices of those SNRs without reported radio spectral indices.

given their radio spectra, regardless of the GeV emission mechanism. The three young SNRs in blue are most consistent with a single underlying particle population, and it has been suggested they emit via IC (dashed line) at GeV energies. SNRs emitting via a combination of mechanisms under these simple assumptions would have indices falling between the two index relations, that is, they would lie in the region spanned by the π^0/bremsstrahlung (solid) and IC (dashed) lines.

The lack of an observed correlation between the indices as expected under these simple assumptions suggests that more detailed physical models are required for the majority of SNR candidates. The observed soft GeV spectra relative to the radio has several potential explanations. The underlying leptonic and hadronic populations

may have different PL indices. The emitting particle populations may not follow a PL but may instead have breaks or even differing spectral shapes. Finally, there may be different zones with different properties dominating the emission at different wavelengths.

In the SNRcat, we also compared the GeV and TeV properties of SNRs to test the second common assumption in SNR models: that momentum distributions of the emitting particle populations do not follow simple PLs but have curvature or breaks. Such changes in spectral slope could also cause breaks in the γ-ray spectra. As TeV emission may originate via the same processes as the *Fermi*-LAT-observed GeV emission (e.g. Funk et al. 2008; Tam et al. 2010; Tibolla 2009), we might expect to see such a change reflected in a spectrum combining *Fermi*-LAT data with observations from iacts such as the High Energy Stereoscopic System (H.E.S.S.), the Very Energetic Radiation Imaging Telescope Array System (VERITAS), and the Major Atmospheric Gamma-ray Imaging Cherenkov telescopes (MAGIC). The converse is also true, where detection predictions in the GeV based on simple PL extrapolation from the TeV have been borne out in GeV studies, e.g. identifications of H.E.S.S. sources from Tibolla (2009) in 2FGL (Nolan et al. 2012) and Ackermann et al. (2012a).

In Figure 5.14 we plot the PL index in the GeV versus TeV range for all SNRs observed with both *Fermi*-LAT and an IACT detections. Six of the ten SNR candidates have TeV indices that are softer than their GeV indices, while three have GeV and TeV indices that are consistent with each other, within statistical and systematic errors. The remaining interacting candidate has a somewhat softer index at GeV energies than at TeV. Such a hardening of the index from GeV to TeV suggests that another particle population may dominate at higher energies or that the emission mechanism may change between the GeV and TeV regimes. Such curvature in

the spectrum may also explain the lack of a simple correlation between GeV and radio PL indices, as described above in this section. We also note that Figure 5.14 shows a distinct separation between young and interacting SNRs, which are often older. This suggests an evolution in index with age, from harder when younger to softer when older.

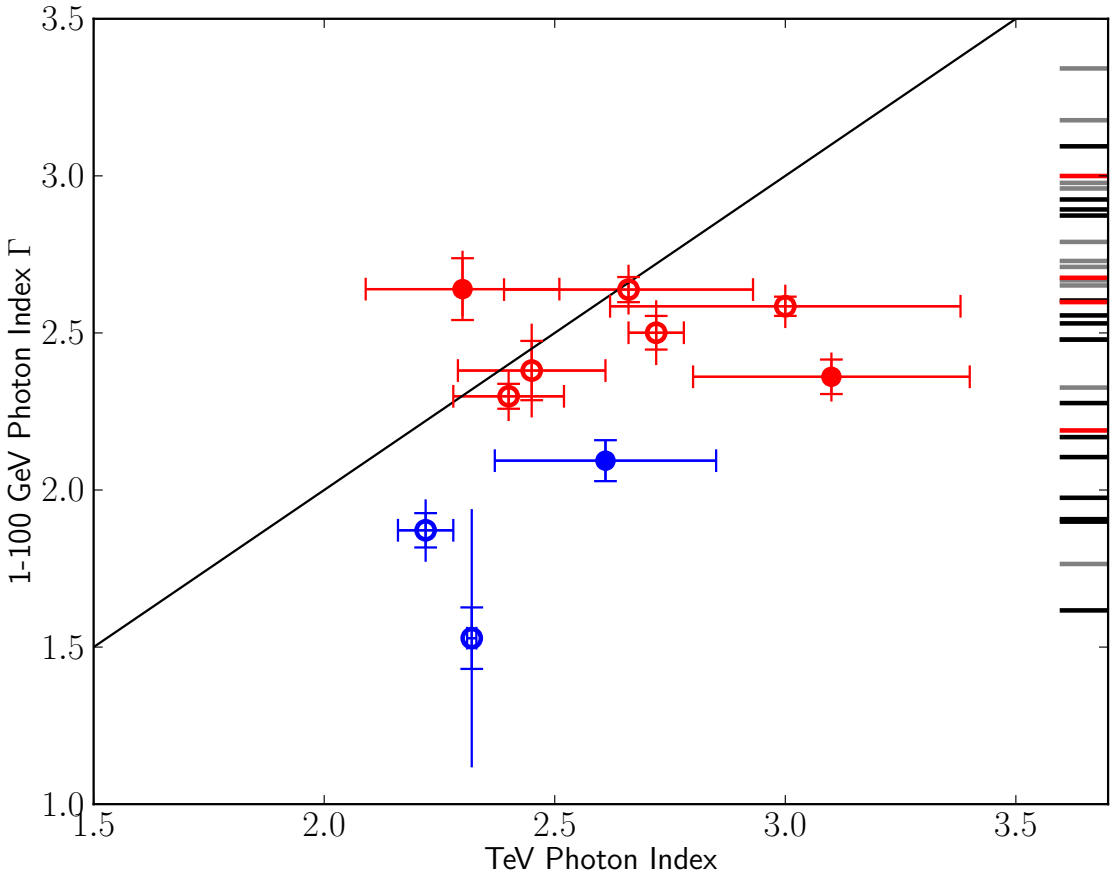

Figure 5.14: GeV index compared to published index measurements from iacts. The line corresponds to equal index values. The predominance of SNRs below the line suggests spectral curvature, potentially reflecting a change in spectral slope of the underlying particle population(s') index or indices. The ticks represent the GeV candidates with indices in the range of those with a TeV counterpart but with no TeV measurements themselves, demonstrating the limitations of the data set. Symbols, colors, and error bars are as in Figure 5.11.

In Figure 5.15, we take SNR ages from the literature and plot the $1 - 100\,\mathrm{GeV}$ photon index versus age. For our uniform sample of all GeV SNR candidates, young

SNRs tend to have harder GeV photon indices than interacting SNRs, which are likely middle aged, though the scatter in age for the two classes is one to two orders of magnitude. The general trend of younger SNRs having harder indices may be due to the decrease of the maximum acceleration energy as SNRs age and their shock speeds slow down. This would also result in fewer particles being swept up by the shock front, given a constant density, suggesting a corresponding decrease in luminosity with age.

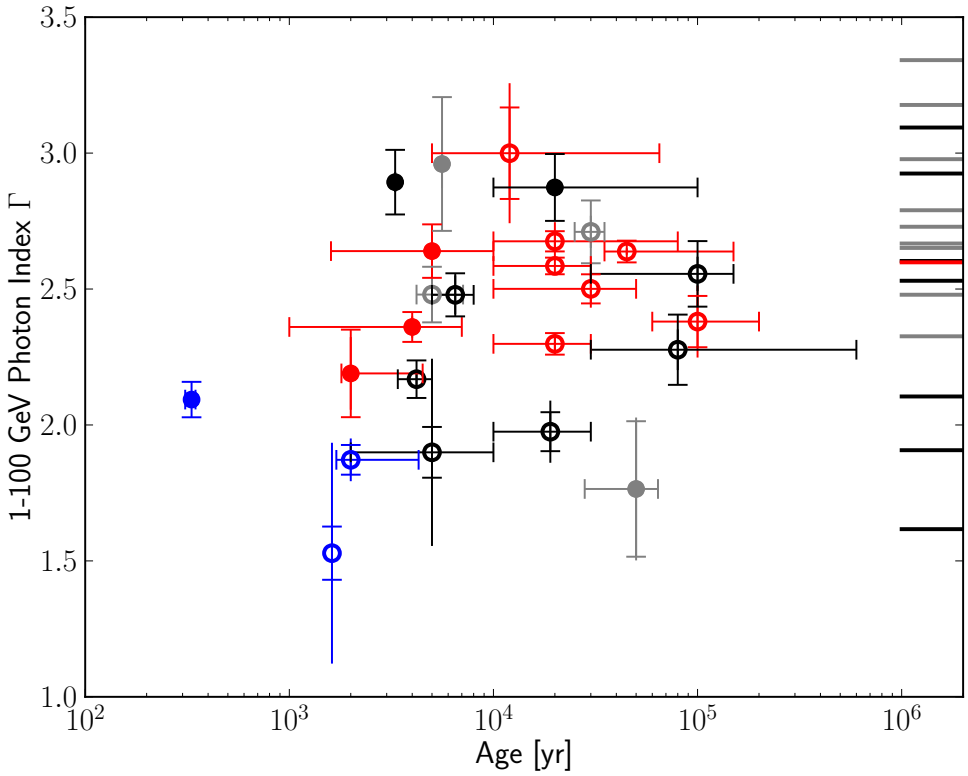

Figure 5.15: Age versus GeV spectral index. For those with ages in the literature, the young (blue) SNR candidates are separated in this phase space from the identified interacting candidates (red). The ticks on the right show indices for GeV candidates without well-established ages. Symbols, colors, and error bars are as in Figure 5.11.

It is important to account for the distances of the SNRs when comparing physical quantities such as luminosity. Table 5.1 records distance from the literature, including the most recent and/or most certain distance estimates adopted in this

work. Of the 279 SNRs studied, only 112 have published distance estimates. Most often these distances are determined from observed line-of-sight velocities using an assumed Galactic rotation curve. Furthermore, kinematic distance estimates have largely been done on an individual basis, and are not uniformly determined for all SNRs. We do not consider distances derived using the "Σ-D relation" because SNRs show a wide range of physical diameters (D) for a given surface brightness (Σ), limiting the utility of such a relationship for determining the distances to individual SNRs (Green 2012).

Table 5.1. Distances to SNRs

Name	d [kpc]	Method	Reference(s)
G000.0+00.0	8.5	IAU value	Kerr & Lynden-Bell (1986)
G000.3+00.0	$8.5^{+3.0}_{-3.0}$	H I	Lang et al. (2010)
G000.9+00.1	$8.5^{+7.5}_{-1.5}$	PSR	Camilo et al. (2009b)
G001.0−00.1	8.5	Maser	Yusef-Zadeh et al. (1999)
G001.4−00.1	$8.5^{+5.6}_{-0.0}$	Maser	Yusef-Zadeh et al. (1999)
G004.5+06.8	$7.0^{+2.0}_{-0.6}$	H I	Reynoso & Goss (1999), Sankrit et al. (2005), Aharonian et al. (2008)
G005.4−01.2	$4.75^{+0.45}_{-0.45}$	Maser	Hewitt & Yusef-Zadeh (2009)
G005.7−00.0	$8.4^{+5.3}_{-5.3}$	Maser	Hewitt & Yusef-Zadeh (2009)
G006.4−00.1	$1.9^{+0.4}_{-0.4}$	Maser, CO	Velázquez et al. (2002)
G008.7−00.1	4.5	Maser	Kassim & Weiler (1990)
G009.7−00.0	4.7	Maser	Hewitt & Yusef-Zadeh (2009)
G011.2−00.3	$5^{+21}_{-0.5}$	H I	Radhakrishnan et al. (1972), Becker et al. (1985), Green et al. (1988)
G012.8−00.0	$4.7^{+1.3}_{-1.1}$	PSR	Halpern et al. (2012)
G013.3−01.3	$3.3^{+1.8}_{-1.7}$	CO	Seward et al. (1995), Koralesky et al. (1998)
G015.1−01.6	$5.7^{+1.3}_{-3.5}$	NH	Boumis et al. (2008)
G015.4+00.1	$4.8^{+1.0}_{-1.0}$	CO	Castelletti et al. (2013)
G016.7+00.1	$10.0^{+3.7}_{-7.4}$	Maser, CO	Hewitt et al. (2008), Reynoso & Mangum (2000)
G016.8−01.1	$5.1^{+4.6}_{-1.8}$	H I	Sun et al. (2011)
G018.1−00.1	$5.58^{+0.24}_{-0.27}$	H I	Leahy et al. (2014)
G018.6−00.2	$4.6^{+0.6}_{-0.6}$	H I	Johanson & Kerton (2009)
G018.8+00.3	$12.0^{+3.0}_{-5.1}$	H I	Tian et al. (2007b)
G021.5−00.9	$4.7^{+0.4}_{-0.4}$	PSR	Camilo et al. (2006), Tian & Leahy (2008b)
G021.8−00.6	$5.35^{+0.15}_{-0.15}$	CO, PSR	Tian & Leahy (2008b), Zhou et al. (2009)
G023.3−00.3	$4.2^{+0.3}_{-0.3}$	H I, CO	Leahy & Tian (2008b), Tian et al. (2007c)
G027.4+00.0	$8.5^{+0.6}_{-1.0}$	H I	Tian & Leahy (2008a)
G028.6−00.1	$7.0^{+1.5}_{-1.0}$	H I, NH	Bamba et al. (2001)
G028.8+01.5	4.0	NH	Schwentker (1994), Misanovic et al. (2010)
G029.7−00.3	$7.8^{+2.8}_{-2.7}$	H I	Leahy & Tian (2008a)
G031.9+00.0	7.2	Maser	Frail et al. (1996)
G032.4+00.1	17	NH	Yamaguchi et al. (2004)
G032.8−00.1	$5.2^{+1.5}_{-0.4}$	Maser	Zhou & Chen (2011)
G033.6+00.1	$7.0^{+1.0}_{-0.5}$	H I	Giacani et al. (2009), Frail & Clifton (1989)
G034.7−00.4	3.0	Maser	Paron et al. (2009)
G035.6−00.4	$3.6^{+0.4}_{-0.4}$	H I	Zhu et al. (2013)
G039.2−00.3	$6.5^{+6.0}_{-0.3}$	CO	Hewitt et al. (2009a), Su et al. (2011)
G041.1−00.3	$10.3^{+2.5}_{-3.9}$	CO	Jiang et al. (2010)
G043.3−00.2	10^{+2}_{-2}	H I	Brogan & Troland (2001)
G049.2−00.7	$4.3^{+1.7}_{-0.0}$	Maser, H I	Koo & Moon (1997), Hewitt et al. (2009b), Tian & Leahy (2013)
G054.1+00.3	$7^{+2.0}_{-2.5}$	H I	Leahy et al. (2008)
G054.4−00.3	$3.0^{+0.8}_{-0.8}$	CO	Junkes et al. (1992), Caswell (1985)
G069.0+02.7	$1.5^{+0.6}_{-0.4}$	H I, PSR	Leahy & Ranasinghe (2012)
G073.9+00.9	$1.3^{+0.7}_{-0.8}$	NH	Lozinskaya et al. (1993)
G074.0−08.5	$0.58^{+0.06}_{-0.06}$	PM	Blair et al. (2009)
G074.9+01.2	$6.1^{+0.9}_{-0.9}$	H I	Kothes et al. (2003)
G076.9+01.0	$10.0^{+5.0}_{-4.0}$	NH	Arzoumanian et al. (2011)
G078.2+02.1	$2^{+2.0}_{-1.5}$	H I	Leahy et al. (2013), Ladouceur & Pineault (2008)
G089.0+04.7	$1.7^{+1.3}_{-1.0}$	CO	Byun et al. (2006)
G106.3+02.7	$0.8^{+1.2}_{-0.1}$	H I	Kothes et al. (2001)
G109.1−01.0	$3.2^{+0.2}_{-0.2}$	H I, CO	Kothes & Foster (2012)
G111.7−02.1	$3.4^{+0.3}_{-0.1}$	PM	Reed et al. (1995)
G114.3+00.3	$1.0^{+1.5}_{-0.3}$	H I	Yar-Uyaniker et al. (2004)
G116.5+01.1	1.6	H I	Yar-Uyaniker et al. (2004)
G116.9+00.2	$1.6^{+1.9}_{-0.0}$	H I	Yar-Uyaniker et al. (2004), Hailey & Craig (1994)
G119.5+10.2	$1.4^{+0.3}_{-0.3}$	H I	Pineault et al. (1993)
G120.1+01.4	$3.0^{+2.0}_{-0.6}$	H I	Tian & Leahy (2011), Hayato et al. (2010), Krause et al. (2008)
G127.1+00.5	$1.15^{+0.35}_{-0.25}$	H I	Pauls (1977), Xilouris et al. (1993), Leahy & Tian (2006)
G132.7+01.3	$2.2^{+0.2}_{-0.2}$	H I	Routledge et al. (1991)

To investigate the role of environment in the trends for the young and interacting SNRs, we examined the GeV luminosity versus radio diameter in Figure 5.16. The square of the physical diameter (D) can be regarded as a reasonable indicator for SNR age and environment (see 2.2), as its evolution during the Sedov-Taylor phase follows

$$D \propto n_0^{-1/5} \; E_{\rm SN}^{1/5} \; t^{2/5} \tag{5.7}$$

where n_0 is the ambient density of the surrounding medium, $E_{\rm SN}$ is the supernova energy, and t is the age of the SNR (Sedov 1959; Taylor 1950). We can thus use the physical diameter as an age proxy: "effective age". Any apparent correlation between the luminosity and D^2 may be due to their inherent dependence on distance (squared). As observed in earlier works, e.g. Thompson et al. (2012), Figure 5.16 shows that, for the detected candidates, interacting SNRs are generally more luminous for a given physical diameter than young SNRs, though there is large scatter. This suggests that SNRs at the same effective age may be more luminous because they have encountered denser gas (n_0). It should also be noted that there is an explicit correlation between the luminosity and physical diameter plotted in Figure 5.16 as both are proportional to distance (squared), which is only reliably measured for a subset of our sample. Observational biases, including that young, often smaller and fainter SNRs tend to be more difficult to detect in the radio as well as in γ-ray, may also affect the observed trends.

[JAM: didn't add anything about maximal CR energy content of all SNRs assuming purely hadronic emission, maybe don't need to]

Table 5.1 (cont'd)

Name	d [kpc]	Method	Reference(s)
G156.2+05.7	$1.1^{+1.9}_{-0.8}$	NH	Pfeffermann et al. (1991), Gerardy & Fesen (2007)
G160.9+02.6	$0.8^{+3.2}_{-0.4}$	H I	Leahy & Tian (2007), Leahy & Roger (1991)
G166.0+04.3	$4.5^{+1.5}_{-1.5}$	H I	Landecker et al. (1989)
G180.0−01.7	$1.3^{+0.22}_{-0.16}$	PSR	Sallmen & Welsh (2004), Ng et al. (2007), Chatterjee et al. (2009)
G184.6−05.8	$1.93^{+0.57}_{-0.43}$	PM	Trimble (1973)
G189.1+03.0	1.5	Maser	Hewitt et al. (2006)
G205.5+00.5	$1.5^{+0.1}_{-0.7}$	H I	Odegard (1986), Fesen et al. (1985), Xiao & Zhu (2012)
G260.4−03.4	$2.2^{+0.3}_{-0.2}$	H I	Dubner & Arnal (1988), Paron et al. (2008)
G263.9−03.3	$0.287^{+0.017}_{-0.021}$	PSR	Moriguchi et al. (2001), Caraveo et al. (2001), Dodson et al. (2003)
G266.2−01.2	$0.75^{+0.15}_{-0.25}$	PM	Katsuda et al. (2008)
G272.2−03.2	$4.0^{+1.0}_{-2.2}$	NH	Lopez et al. (2011)
G284.3−01.8	3	CO	Ruiz & May (1986)
G290.1−00.8	$7^{+4.0}_{-3.5}$	H I	Rosado et al. (1996a), Slane et al. (2002), Reynoso et al. (2006)
G291.0−00.1	$5^{+1}_{-1.5}$	NH	Harrus et al. (1998)
G292.0+01.8	$6.2^{+0.9}_{-0.9}$	H I, PSR	Gaensler & Wallace (2003)
G292.2−00.5	$8.4^{+0.4}_{-0.4}$	PSR	Caswell et al. (2004), Camilo et al. (2000)
G296.5+10.0	$2.1^{+1.8}_{-0.9}$	H I	Giacani et al. (2000)
G304.6+00.1	$9.7^{+4.3}_{-1.7}$	H I	Caswell et al. (1975)
G308.4−01.4	$9.8^{+0.0}_{-3.9}$	NH	Prinz & Becker (2012)
G309.2−00.6	$4.0^{+1.4}_{-2.0}$	NH	Rakowski et al. (2001)
G315.1+02.7	$1.7^{+3.7}_{-0.3}$	PM	Stupar et al. (2007)
G315.4−02.3	$2.5^{+0.3}_{-0.2}$	PM	Rosado et al. (1996a), Sollerman et al. (2003a)
G315.9−00.0	8^{+2}_{-2}	PSR	Camilo et al. (2009a)
G316.3−00.0	$7.2^{+22.8}_{-2.5}$	H I	Caswell et al. (1975)
G318.2+00.1	$4.0^{+5.4}_{-0.7}$	H I	Hofverberg et al. (2010)
G320.4−01.2	$5.2^{+1.4}_{-1.4}$	H I, NH	Gaensler et al. (1999)
G321.9−00.3	$6^{+4.0}_{-0.5}$	H I	Stewart et al. (1993)
G326.3−01.8	$4.1^{+0.7}_{-0.7}$	NH	Rosado et al. (1996a), Kassim et al. (1993)
G327.1−01.1	$6.5^{+6.5}_{-1.5}$	NH	Sun et al. (1999)
G327.4+00.4	4.3	H I	McClure-Griffiths et al. (2001)
G327.6+14.6	$2^{+0.2}_{-0.4}$	PM	Nikolić et al. (2013)
G328.4+00.2	$17.4^{+2.6}_{-5.4}$	H I	McClure-Griffiths et al. (2001)
G330.2+01.0	4.9	H I	McClure-Griffiths et al. (2001)
G332.4−00.4	3.3	H I, CO	Paron et al. (2006), Reynoso et al. (2004)
G332.4+00.1	$7.5^{+3.5}_{-4.2}$	NH	Vink (2004)
G335.2+00.1	1.8	CO	Eger et al. (2011)
G337.0−00.1	11.0	Maser	Frail et al. (1996)
G337.2+00.1	$14.0^{+16.0}_{-0.5}$	H I, NH	Combi et al. (2005), Combi et al. (2006)
G337.2−00.7	$5.8^{+3.8}_{-3.8}$	H I	Rakowski et al. (2006), Lopez et al. (2011)
G337.8−00.1	12.3	Maser	Frail et al. (1996)
G338.3−00.0	$10.0^{+3.0}_{-2.0}$	H I	Lemiere et al. (2009)
G343.0−06.0	$1.0^{+0.5}_{-0.5}$	H I, NH	Kim et al. (2010), Welsh et al. (2003), Walker & Zealey (2001)
G346.6−00.2	11.0	Maser	Frail et al. (1996)
G347.3−00.5	$1.0^{+0.3}_{-0.2}$	H I, CO	Moriguchi et al. (2005)
G348.5+00.1	$9^{+0.5}_{-2.7}$	H I	Tian & Leahy (2012)
G348.5−00.0	$6.3^{+7.4}_{-3.3}$	Maser	Tian & Leahy (2012)
G348.7+00.3	13.2	H I	Tian & Leahy (2012)
G349.7+00.2	$11.5^{+0.7}_{-0.7}$	Maser	Frail et al. (1996), Tian & Leahy (2014)
G350.1−00.3	$4.5^{+6.2}_{-0.5}$	H I	Gaensler et al. (2008)
G351.7+00.8	$13.2^{+0.5}_{-11.1}$	H I	Tian et al. (2007a)
G352.7−00.1	$7.5^{+0.9}_{-0.7}$	H I, CO	Giacani et al. (2009)
G353.6−00.7	$3.2^{+0.8}_{-0.8}$	H I, CO	Tian et al. (2008)
G357.7+00.3	6.9	Maser	Frail et al. (1996)
G357.7−00.1	12	Maser	Frail et al. (1996), Gaensler et al. (2003), Lazendic et al. (2004)
G359.1−00.5	4.6	Maser	Yusef-Zadeh et al. (2007), Hewitt et al. (2008)

Note. — Table of SNR distances drawn from the literature. The method for determining the distance is noted as: CO = line-of-sight velocity from molecular CO lines; H I = kinematic distance from H I absorption; NH = extinction estimate from optical or X-rays; Maser = kinematic distance from OH maser velocity; PM = Proper motions; PSR = association with pulsar. The d_{error} values indicate the range of uncertainties from the quoted distance values as assessed in the cited publications. The distance uncertainties are often asymmetric.

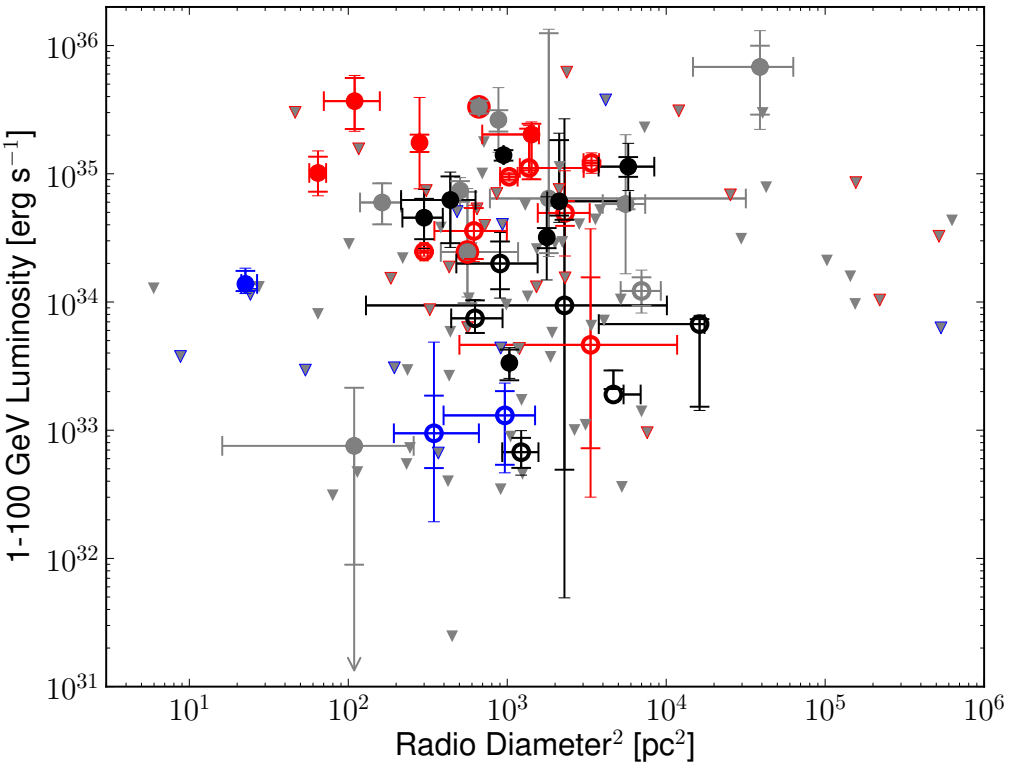

Figure 5.16: [The $1-100$ GeV luminosity vs. D^2] The $1-100$ GeV luminosity is plotted against the square of the radio diameters in pc of those SNRs with known distances. Symbols, colors, and error bars are as in Figure 5.11.

5.11 Conclusions

In this Chapter, we have discussed the state of γ-ray observations of SNRs prior to the launch of *Fermi*, and the unique role that the LAT plays in identifying SNRs and exploring γ-ray production mechanisms therein. We presented the new automated source addition and analysis method, `addSrcs`, and its application to studying the population of SNRs emitting GeV γ-rays, published in Acero et al. (2016). With this first *Fermi*-LAT SNR Catalog we have systematically characterized GeV emission in regions containing known radio SNRs, creating new methods to address issues associated with these typically complex regions. These include methods for system-

atically adding sources to a region and better estimating the systematic error due to choice of interstellar emission model (discussed in detail in)Acero et al. (2016)). From this, we have determined characteristics of the GeV SNR population, down to our measurement limit, finding 30 classified and 14 marginal candidates with a false identification limit of <22%(Acero et al. 2016). This GeV data provide a crucial context for the detailed modeling of individual SNRs. In combination with multiwavelength measurements, the GeV data now challenge simple, previously sufficient SNR emission models. Within the limits of existing multiwavelength data, our observations generally support previous findings of changes in spectral slope at or near TeV energies and a softening and brightening in the GeV range with age and effective age, yet we see indications that new candidates and new multiwavelength data may provide evidence of exceptions to this trend.

[JAM: EGRET point source sensitivity is $\sim$ 1x10^{-7} cm^{-2} s^{-1} `http://fermi.gsfc.nasa.gov/science/instruments/table1-1.html` get this number from some paper instead?]

[JAM: Another pointlike assumption to speed things up is that the PSF doesn't vary too much with event incidence angle in individual bins. To ensure this even more, events with a reconstructed angle ¿ 66.4deg (cos theta = 0.4) are removed (idk why this angle)]

[JAM: I did work for mock catalog, but it was really just running addsrcs centered on the mock positions]

Chapter 6

Extended Source Detection above 50 GeV: The 2FHL Catalog

Application of addSrcs searching for extended (and really point too) sources in the sky. 2FHL results on all Galactic sources. Index histograms for entire Second Catalog of Hard Fermi-LAT Sources (2FHL)population showing harder index for Galactic sources.

We don't just detect extended though! The pipeline was built to try extended and if that's not likely, revert to point source. Simple check with Alberto's pipeline to show we didn't detect any glaring discrepancies. Quick check of Alberto's results for clusters of point source at $|b| < 10^{\circ}$.

How much of the 2FHL paper can I put in as is, how much can I take with modifications?

Below is if I just took the sections describing extend sources.

Something about connecting to TeV

6.1 Extended Sources Previously Detected by the LAT

We explicitly modeled sources as spatially extended when a previous, dedicated, analysis found the source to be resolved by the LAT. The 25 extended sources reported in 3FGL were included in our model using the spatial templates derived in the individual source studies (see references in Acero et al. 2015). Refitting the positions and extensions of the 3FGL extended sources in this energy range is beyond the scope of this work.

Of the 25 3FGL extended sources, 19 are significantly detected here above the detection threshold (TS $\geq$ 25). Only 6 sources are not detected and, since all have TS $<$ 10, are removed from the sky model (see §6.3 for details).

One extended LAT source has had a dedicated analysis published since the release of the 3FGL catalog. Abramowski et al. (2015a) reported joint H.E.S.S. and LAT observations of the very high energy (VHE) source HESS J1834-087. This source is coincident with supernova remnant (SNR) W41 and was detected as spatially extended in a wide energy range spanning 1.8 GeV to 30 TeV. In this paper, we employ the spatial model for the GeV emission determined in Abramowski et al. (2015a), leading to a significant detection of this source.

6.2 Newly Detected Extended Sources

In addition to modeling the extended sources mentioned in §6.1, we performed a blind search of the Galactic plane ($|b| < 10^\circ$) to identify potential extended sources not included in previously published works. Our analysis pipeline is similar to that used in Hewitt et al. (2013), with some modifications tailored to searching for

multiple extended sources in an ROI. The pipeline employs the `pointlike` binned maximum likelihood package (Kerr 2010), in particular utilizing the extended source fitting tools validated by Lande et al. (2012) to simultaneously fit the position, extension, and spectra of sources in our ROI.

We created 72 ROIs of radius 10°, centered on $b = 0°$ with neighboring ROIs overlapping and separated by 5° in Galactic longitude. Our initial model of the γ-ray emission in each ROI consisted solely of the Galactic diffuse (allowing just the normalization to be fit) and isotropic emission models (fixing the normalization), with no other sources in the ROI. Emission in the ROIs was further characterized by adding sources and fitting their spectral parameters (normalization and spectral index) in a $14° \times 14°$ region.

A TS map, that included all significant sources found previously, made up of $0.1° \times 0.1°$ bins across the ROI, was created at each iteration and a small radius (0.1°) uniform disk, with a power-law spectrum was placed at the position of the peak TS pixel. The spectra of any newly added sources, as well as the position, extension, and spectral parameters of the disk were then fit. If $TS_{ext} \geq 16$, where $TS_{ext} = 2 \log(\mathcal{L}_{ext}/\mathcal{L}_{ps})$ (i.e.twice the logarithm likelihood ratio of an extended to a point source, Lande et al. 2012), then the disk was kept in the model. For $TS_{ext} < 16$, the extended source was replaced by a point source with a power-law spectral model. For the point-source replacement case, spectral parameters of sources in the ROI were fit and the position of the new point source was optimized. Finally, the spatial parameters of any previously added extended sources were refit iteratively before creating a new TS map and repeating the process. We stopped adding sources when the peak TS was less than 16 for two successive sources.

To assess the impact of fitting extended sources when starting with an ROI devoid of sources, a crosscheck analysis (also using `pointlike`) was performed across

the Galactic plane. We included 3FGL point and extended sources, the Galactic diffuse and isotropic emission, and pulsars from the second LATpulsar catalog (Abdo et al. 2013) (as well as from 3FGL) in the preliminary source model for each region. Sources were iteratively added to account for residual emission and both these residual sources and 3FGL sources were tested for extension. Remarkably, this alternative analysis converges (i.e.spectral and spatial parameters for the detected extended sources are compatible in both analyses) to the initially source-devoid analysis for nearly all detected extended sources.

Extended sources detected in the analysis described in this section for which the position and extension were compatible with those found by the crosscheck were included in the ROI model at step 1 of the full ML analysis detailed in §**??**. Seed point sources interior to the extended sources were removed prior to the ML fit. To address the ambiguity between detecting a source as spatially extended as opposed to a combination of point sources, we utilized the algorithm detailed in Lande et al. (2012) to simultaneously fit the spectra and positions of two nearby point sources. We only consider a source to be extended if $\mathrm{TS_{ext}} > \mathrm{TS_{2pts}}$ (improvement when adding a second point source). Our blind search of the Galactic plane allowed us to find 5 sources not previously detected as extended by *Fermi*-LAT. Further details on these sources are presented in § 6.3.

6.3 Extended Source Results

In total, 31 sources are modeled as spatially extended and input into the ML analysis: 25 listed in 3FGL, 5 sources detected in the `pointlike` analysis (described in § 6.1) that were not detected as extended at the time of 3FGL, and one, SNR W41, reported recently by both the H.E.S.S. and LAT teams (Abramowski et al. 2015a).

Names and properties of the extended sources are provided in Tables 6.1 and 7.2. Six extended sources, detected in 3FGL, were not detected in 2FHL: the SMC, S 147 (the point source 2FHL J0534.1+2753 was detected inside it), the lobes of Centaurus A (although we detect its core as a point source, 2FHL J1325.6−4301), W 44, HB 21 and the Cygnus Loop.

We detect a weak source, 2FHL J1714.1−4012 (TS = 27), just outside the south-western edge of the 3FGL spatial template used to model the emission from SNR RX J1713.7−3946 (2FHL J1713.5−3945e). 2FHL J1714.1−4012 has a hard spectral index $\Gamma = 1.63 \pm 0.38$, that is within errors of the spectral index derived for the SNR, $\Gamma = 2.03 \pm 0.20$. It is unclear whether 2FHL J1714.1−4012 is a distinct source separated from the SNR, or the result of un-modeled residual emission due to an imperfection in the spatial template adopted for the extended source.

2FHL J1836.5−0655e is associated with the PWN HESS J1837−069. The 3FGL catalog contains several point sources in the vicinity of the PWN. We detect three sources in the vicinity, 2FHL J1834.5−0701, 2FHL J1837.4−0717 and 2FHL J1839.5−0705, the first two of which are coincident with 3FGL sources (3FGL J1834.6−0659, 3FGL J1837.6−0717 respectively). The power-law spectral indices of the three 2FHL point sources and 2FHL J1836.5−0655e are all consistent with each other. The concentration of sources around HESS J1837−069 combined with the spectral compatibility of the sources is suggestive of a common origin to the γ-ray emission in this region. However, the surrounding γ rays could arise from other sources in the region (Gotthelf & Halpern 2008); further analysis is necessary to determine the nature of the sources in this region.

A brief description of the five new 2FHL extended sources is given below with residual TS maps for the region surrounding each source shown in Figure 6.1. Detailed analyses of these new extended sources will be reported in separate papers.

2FHL J1443.2−6221e overlaps with the young, radio-detected SNR RCW 86 (G315.42.3). RCW 86 is a 42′ diameter SNR that lies at a distance of 2.3-2.8 kpc and is likely associated with the first recorded supernova, SN 185 AD (Rosado et al. 1996b; Sollerman et al. 2003b). With more than 40 months of data and using the `P7SOURCE` dataset, the LAT did not significantly detect the SNR, but upper limits on detection at GeV energies combined with detection of significant extension in the TeV (Aharonian et al. 2009) were sufficient to strongly favor a leptonic origin for the emission (Lemoine-Goumard et al. 2012).

An updated LAT analysis of RCW 86 using 76 months of data, as well as the Pass 8 event-level analysis, resulted in detection of the SNR by the LAT as well as significant extension measurement (Hewitt & Lemoine-Goumard 2015). In this paper, we report the results derived for 2FHL J1443.2−6221e from the `pointlike` analysis described in § 6.1.

2FHL J1419.2−6048e is a newly detected extended sources with size $\sigma_{\rm disk} = 0.36^\circ \pm 0.03^\circ$, that overlaps two nearby PWN/PSR complexes in the Kookaburra region. In the southwest of Kookaburra, HESS J1418−609 (Aharonian et al. 2006) is coincident with both the extended non-thermal X-ray "Rabbit" PWN (G313.3+0.1, Roberts et al. 1999), and the γ-ray detected pulsar PSR J1418−6058 (Abdo et al. 2009). The northeast region, called "K3", contains HESS J1420−607, coincident with PWN G313.5+0.3 and PSR J1420−6048. Acero et al. (2013) detected, with LAT, emission from both HESS J1418−609 (with a soft spectral index, pulsar-like spectrum) and HESS J1420−607 (with a hard power-law index) above 10 GeV, but only HESS J1420−607 was significantly detected above 30 GeV. Neither showed significant extension. Our result for the fitted power-law spectral index of 2FHL J1419.2−6048e is in agreement with the previous GeV and TeV results, yet our measured radius is considerably larger than the TeV extension. To compare the ex-

tensions of the uniform disk model used for 2FHL J1419.2−6048e in this paper to the Gaussian model of Aharonian et al. (2006), we defined the radius which contains 68% of the source's intensity as r_{68}, with $r_{68,\mathrm{Gaussian}} = 1.51\sigma$, and $r_{68,\mathrm{disk}} = 0.82\sigma$ (Lande et al. 2012). We find that $r_{68} \simeq 0.30^\circ$ for 2FHL J1419.2−6048e, and $r_{68} \simeq 0.09^\circ$ for HESS J1420−607.

2FHL J1355.2−6430e, coincident with the VHE source HESS J1356−645, is detected as extended ($\sigma_{\mathrm{disk}} = 0.57^\circ \pm 0.02^\circ$) for the first time by the LAT in this work. The source HESS J1356−645 (Abramowski et al. 2011) is associated with the pulsar PSR J1357−6429, which was determined to be powering a surrounding extended radio and X-ray PWN (Lemoine-Goumard et al. 2011). Acero et al. (2013) detected faint emission from the nebula, and derived a 99% c.l. Bayesian upper limit on extension ($\sigma_{\mathrm{Gauss}} < 0.39^\circ$) in the absence of significant extension. The fitted spectral index for 2FHL J1355.2−6430e is compatible with the GeV and TeV results (Abramowski et al. 2011; Acero et al. 2013), however, the fitted disk extension is larger than that of the TeV detection, with $r_{68} \simeq 0.47^\circ$ for 2FHL J1355.2−6430e and $r_{68} \simeq 0.30^\circ$ for HESS J1356−645.

2FHL J1112.4−6059e is an extended source ($\sigma_{\mathrm{disk}} = 0.53^\circ \pm 0.03^\circ$) newly detected by the LAT that encircles two 3FGL sources, 3FGL J1111.9−6058 and 3FGL J1111.9−6038, and has another, 3FGL J1112.0−6135, just outside its boundary (Acero et al. 2015). The extended source also partially overlaps the massive star forming region NGC 3603.

Finally, **2FHL J0431.2+5553e** is a large extended source ($\sigma_{\mathrm{disk}} = 1.27^\circ \pm 0.04^\circ$), with a hard spectrum, that has not been previously detected at γ-ray energies. It overlaps the recently discovered radio SNR G150.3+4.5 (Gao & Han 2014). G150.3+4.5 is a $2.5^\circ \times 3^\circ$ (Galactic coordinates) elliptical shell type SNR that has a steep radio synchrotron spectrum ($\alpha = -0.6$), indicative of radio SNRs.

Table 6.1. 2FHL extended sources previously detected by the *Fermi*-LAT

2FHL Name	l [deg]	b [deg]	TS	Association	Class	Spatial model	Extension [deg]
J0526.6−6825e	278.843	-32.850	49.80	LMC	gal	2D Gaussian	1.87
J0617.2+2234e	189.048	3.033	398.64	IC 443	snr	2D Gaussian	0.27
J0822.6−4250e	260.317	-3.277	63.87	Puppis A	snr	Disk	0.37
J0833.1−4511e	263.333	-3.104	49.70	Vela X	pwn	Disk	0.91
J0852.8−4631e	266.491	-1.233	437.21	Vela Jr	snr	Disk	1.12
J1303.4−6312e	304.235	-0.358	56.06	HESS J1303−631	pwn	2D Gaussian	0.24
J1514.0−5915e	320.269	-1.276	165.51	MSH 15−52	pwn	Disk	0.25
J1615.3−5146e	331.659	-0.659	128.15	HESS J1614−518	spp	Disk	0.42
J1616.2−5054e	332.365	-0.131	87.18	HESS J1616−508	pwn	Disk	0.32
J1633.5−4746e	336.517	0.121	114.17	HESS J1632−478	pwn	Disk	0.35
J1713.5−3945e	347.336	-0.473	60.98	RX J1713.7−3946	snr	Map	0.56
J1801.3−2326e	6.527	-0.251	50.20	W 28	snr	Disk	0.39
J1805.6−2136e	8.606	-0.211	160.43	W 30	snr	Disk	0.37
J1824.5−1350e	17.569	-0.452	266.09	HESS J1825−137	pwn	2D Gaussian	0.75
J1834.9−0848e	23.216	-0.373	67.30	W 41	spp	2D Gaussian	0.23
J1836.5−0655e	25.081	0.136	62.72	HESS J1837−069	pwn	Disk	0.33
J1840.9−0532e	26.796	-0.198	163.15	HESS J1841−055	pwn	Elliptical 2D Gaussian	0.62, 0.38, 39
J1923.2+1408e	49.112	-0.466	44.60	W 51C	snr	Elliptical Disk	0.38, 0.26, 90
J2021.0+4031e	78.241	2.197	115.97	Gamma Cygni	snr	Disk	0.63
J2028.6+4110e	79.601	1.396	28.09	Cygnus Cocoon	sfr	2D Gaussian	3.0

Note. — List of the 20 extended sources in the 2FHL that were previously detected as extended by the *Fermi*-LAT. All these sources are in 3FGL except W41, which is studied by Abramowski et al. (2015b). The Galactic coordinates l and b are given in degrees. The extension of the disk templates is given by the radius, the extension of the 2D Gaussian templates is given by the 1σ radius, and the elliptical templates are given by the semi-major axis, semi-minor axis, and position angle (East of North).

6.4 Summary

In this chapter, we have presented the publication on 2FHL, focusing primarily on the Galactic results of the publication and in particular detected extended sources. Extension of addSrcs to search for spatially extended sources, applied to 8 years [JAM: check] of LAT data above 50 GeV. Detected x extended. y were known 3FGL, z were new;y detected as extended at GeV energies, SNR G150.3+4.5 was brand new. Galactic seem to have harder indices than extra gal, suggests which unid'd in the plane are gal vs. egal. All extended harder than diffuse. Hints of different morphology between 2FHLand 2FGL, didn't study here, but this is one of the motivations for >10 GeVstudy.

Table 6.2. New 2FHL extended sources

2FHL Name	l [deg]	b [deg]	TS	TS_{ext}	TS_{2pts}	F_{50}	ΔF_{50}	Γ	$\Delta\Gamma$	Association	Class	Radius [deg]
J0431.2+5553e	150.384	5.216	87.9	83.4	26.2	11.70	2.11	1.66	0.20	G 150.3+4.5	snr	1.27
J1112.4−6059e	291.222	-0.388	80.9	68.3	22.5	12.80	2.36	2.15	0.28	PSR J1112−6103	pwn	0.53
J1355.2−6430e	309.730	-2.484	82.3	31.8	12.9	9.59	1.95	1.56	0.22	PSR J1357−6429	pwn	0.57
J1419.2−6048e	313.432	0.260	109.3	49.1	15.6	17.60	2.80	1.87	0.19	PSR J1420−6048	pwn	0.36
J1443.2−6221e	315.505	-2.239	75.6	29.9	19.2	7.23	1.70	2.07	0.30	SNR G315.4−2.3	snr	0.27

Note. — List of the 5 new extended sources in the 2FHL. All these sources are characterized by an uniform disk template whose radius is given in the last column.

6.5 Scratch

Add stuff to first section about extension fitting with pointlike In addition to being optimized for speed and large-scale studies (i.e. those including many sources), `pointlike`

I should probably give more detail about Josh's code than I did for just the regular pointlike?

Next, get into Josh's extension additions to pointlike It accomplishes this by binning the sky in

Should I say some things about why extension fitting is important in general?

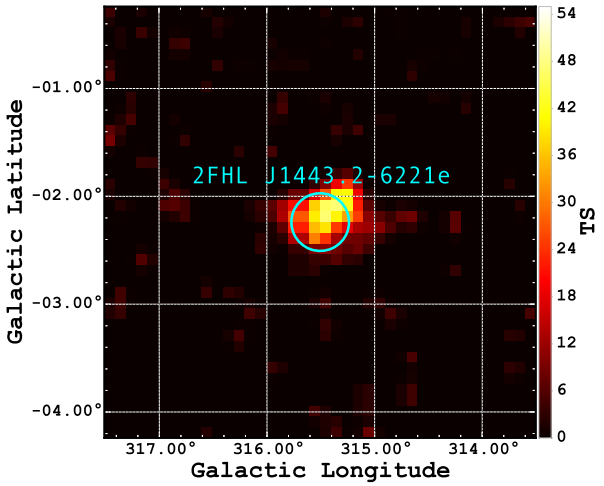
2FHL J1443.2-6221e
Galactic Latitude
-01.00°
-02.00°
-03.00°
-04.00°
317.00°
316.00°
315.00°
314.00°
Galactic Longitude
TS
54
48
42
36
30
24
18
12
6
0

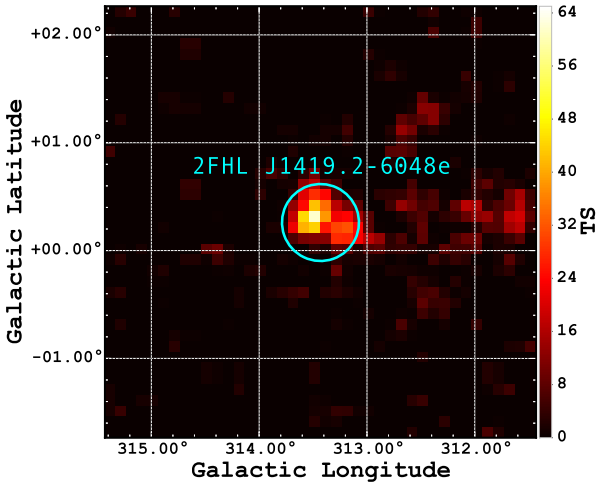
2FHL J1419.2-6048e
Galactic Latitude
+02.00°
+01.00°
+00.00°
-01.00°
315.00°
314.00°
313.00°
312.00°
Galactic Longitude
TS
64
56
48
40
32
24
16
8
0

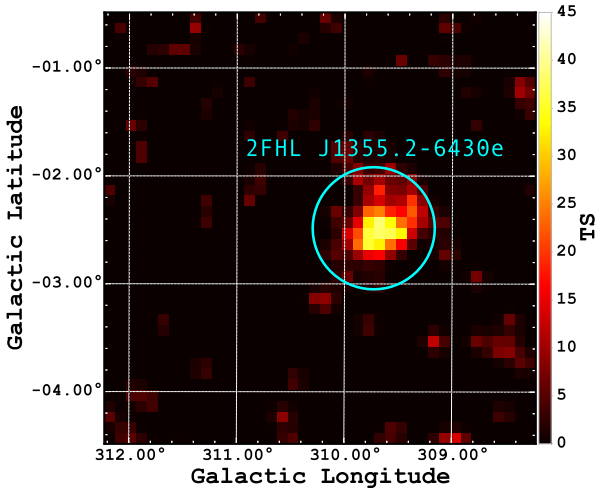
2FHL J1355.2-6430e
Galactic Latitude
-01.00°
-02.00°
-03.00°
-04.00°
312.00°
311.00°
310.00°
309.00°
Galactic Longitude
TS
45
40
35
30
25
20
15
10
5
0

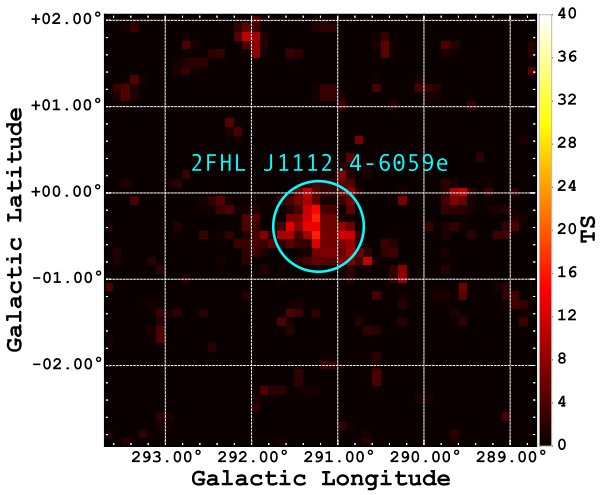
2FHL J1112.4-6059e
Galactic Latitude
+02.00°
+01.00°
+00.00°
-01.00°
-02.00°
293.00°
292.00°
291.00°
290.00°
289.00°
Galactic Longitude
TS
40
36
32
28
24
20
16
12
8
4
0

Chapter 7

SNR G150.3+4.5

Dedicated analysis of one interesting 2FHLresult. First blindly detected extended γ -ray source.

-Direct application of addSrcs to an intersting newly detected GeV SNR

-dedicated analysis of the one source to try to understand its nature

-It's interesting because :

-it was blindly detected

-might be the closest rem

-spectrum + index seems like dynamically young, but age and distance are hard to constrain, so it could be older

-Understanding this remnant contributes to the connection between Fermi and TeV telescopes

Take this all straight from the paper I write. Not sure how much more I'd need to add From the SNR cat, "We also note that one classified extended candidate may be consistent with an IC origin, though no error was reported on the radio spectral index measurement by **?**". What sources is this? is G150 one of the only extended young SNRs? can't be true right? vela JR is young and extended

7.1 Introduction

Supernova remnants have long been thought to be the primary accelerators of cosmic rays up to the knee of the cosmic ray energy spectrum.

what to say about radio SNRs? Connect CRs to nonthermal emission and the LAT and Something about SNRs, cosmic ray accelerators, radio detections, connection between radio-LAT observations, G150 detection, 2FHL blind detection and SNRs at TeV (all young?), this paper extends the energy down to

Focus more on the hadronic vs leptonic since that's what's interesting? We describe the LAT and analysis results in §7.2, detail multiwavelength observations in §7.3, and discuss various emission origin scenarios in §7.4.

7.2 *Fermi*-LAT Observations and Analysis

7.2.1 Data Set and Reduction

Fermi-LATis a pair conversion telescope sensitive to high energy γ-rays from 20 MeV to greater than 1 TeV (Ackermann et al. 2016), operating primarily in a sky-survey mode which views the entire sky every 3 hours. The LAT has wide field of view ($\sim$2.4 sr), a large effective area of $\sim$8200 cm^2 above 1 GeV for on axis events and a 68% containment radius angular resolution of $\sim0.8^\circ$ at 1 GeV. For further details on the instrument and its performance see Atwood et al. (2009) and Ackermann et al. (2012c).

In this analysis, we analyzed 7 years of Pass 8 data, from August 2nd 2008 to August 2nd 2015. The Pass 8 event reconstruction provides a significantly improved angular resolution [JAM: this is sadly unimportant unless I'm at higher energy or using the PSF types. The P8 total PSF at 1 GeV is about the same as for P7REP.

It's the acceptance/effective area that are considerably better at this energy], acceptance, and background event rejection (Atwood et al. 2013a,b), all of which lead to an increase in the effective energy range and sensitivity of the LAT. Source class events were analyzed within a 14°x14° region centered on SNR SNR G150.3+4.5 using the P8R2_SOURCE_V6 instrument response functions, with a pixel size of 0.1°. To reduce contamination from earth limb γ-rays, only events with zenith angle less than 100° were included.

For spectral and spatial analysis we utilized both the standard *Fermi*Science Tools (version 10-01-01)[1] , and the binned maximum likelihood package `pointlike` (Kerr 2010). `pointlike` provides methods for simultaneously fitting the spectrum, position, and spatial extension of a source, and was extensively validated in Lande et al. (2012). Both packages fit a source model, the Galactic diffuse emission, and an isotropic component (which accounts for the background of misclassified charged particles and the extragalactic diffuse γ-ray background)[2] to the observations. In this analysis, we used the standard Galactic diffuse ring-hybrid model scaled for Pass 8 analysis, gll_iem_v06.fits (modulated by a power law function with free index and normalization), and for the isotropic emission, we used iso_P8R2_SOURCE_V6_v06.txt, extrapolated to 2 TeV as in Ackermann et al. (2016).

In our source model for the region, we included sources from the third *Fermi*-LATcatalog (Acero et al. 2015, 3FGL) within 15° of the center of our region of interest (RoI). We replaced the position and spectrum of any 3FGL pulsars in the region with their corresponding counterpart from the LAT 2nd pulsar catalog (Abdo et al. 2013). Residual emission unaccounted for by 3FGL sources is present in the RoI due to the increased time range and different energy selection with respect to that

[1] `http://fermi.gsfc.nasa.gov/ssc/`

[2] `http://fermi.gsfc.nasa.gov/ssc/data/access/lat/BackgroundModels.html`

in 3FGL. We added to the RoI several point sources to account for this unmodeled emission and minimize the global residuals.[JAM: do I need to say more about these sources? should I mention adding them automatially and iteraively based on TS maps and reference SNRcat/2FHL? How close is the closest source? Mention this and use as an argument for not saying much more about them]. The normalization and spectral index of sources within 5° of the center of the RoI were free to vary, whereas all other source parameters were fixed. A preliminary maximum likelihood fit of the RoI was performed, and sources with a test statistic (TS) < 9 (TS is defined as, TS $= 2$ Log$(\mathcal{L}_1/\mathcal{L}_0)$ where $\mathcal{L}_1$ is the likelihood of source plus background and $\mathcal{L}_0$ that of just the background) were removed from the model.

7.2.2 Morphological Analysis

Studying the spatial extension of sources with the LAT is non-trivial due to the energy-dependent point spread function (PSF) and strong diffuse emission present in the Galactic plane. Soft spectrum point sources and uncertainties in the diffuse model can be a source of systematic error when not accurately modeling extended emission as such, particularly at low energies where the PSF is broad. To strike a balance between the best angular resolution and minimal source and diffuse contamination, we restrict our morphological analysis to energies between 1 GeV and 1 TeV. We divide this energy range into 12[JAM: 4bpd] logarithmically spaced bins for both `pointlike` and `gtlike` binned likelihood analyses.

Three unidentified 3FGL sources are located within the extent of SNR G150.3+4.5. 3FGL J0425.8+ 5600, located approximately 0.6° from the center of the SNR, is the closest of the three sources and is described with a power law spectrum of index $\Gamma = 2.35 \pm 0.17$ in the 3FGL catalog. The closest radio source to 3FGL J0425.8+5600 is NVSS J042719+560823, at 0.25 away (Ref?). 3FGL J0423.5+5442,

exhibits a power law spectral index, $\Gamma = 2.63 \pm 0.15$, with no clear multiwavelength source association. Finally, 3FGL J0426.7+5437 has a pulsar-like spectrum, yet in a timing survey performed with the 100-m Effelsberg radio telescope, Barr et al. (2013) were unable to detect pulsations from the source down to a limiting flux density of ~ 0.1 mJy. The source is located about 0.8° from the center of the SNR. We discuss this source and potential association with SNR G150.3+4.5 further in §7.4.2).

In our analysis, we removed 3FGL J0425.8+5600 and 3FGL J0423.5+544 from the RoI, but kept 3FGL J0426.7+5437 in the model since preliminary analyses showed clear positive residual emission at the position of the source if it was removed from the RoI. Figure 7.1 shows a residual TS map for the region around SNR G150.3+4.5. This point source detection-significance map was created by placing a point source modeled with a power law of photon index, $\Gamma = 2$ at each pixel and gives the significance of detecting a point source at each location above the background.

We modeled the excess emission in the direction of SNR G150.3+4.5 with a uniform intensity, radially-symmetric disk, simultaneously fitting the spatial and spectral components of the model via `pointlike`. The extension of the disk was initialized with a seed radius of $\sigma = 0.1°$ and position centered on the radio position of SNR G150.3+4.5. We define the significance of extension as in Lande et al. (2012); $\mathrm{TS_{ext}} = 2\ \log(\mathcal{L}_{\mathrm{ext}}/\mathcal{L}_{\mathrm{ps}})$, with $\mathcal{L}_{ext}$ being the likelihood of the model with the extended source and $\mathcal{L}_{ps}$ that with of a point source located at the peak of emission interior to the extended source. For the disk model, $\mathrm{TS_{ext}} = 298$, with a best fit radius, $\sigma = 1.40° \pm 0.03°$ [JAM: I should just put this all in a table and reference it], which is in excellent agreement with the radio size of the SNR determined in Gao & Han (2014). We tried adding back in to our model the two removed 3FGL

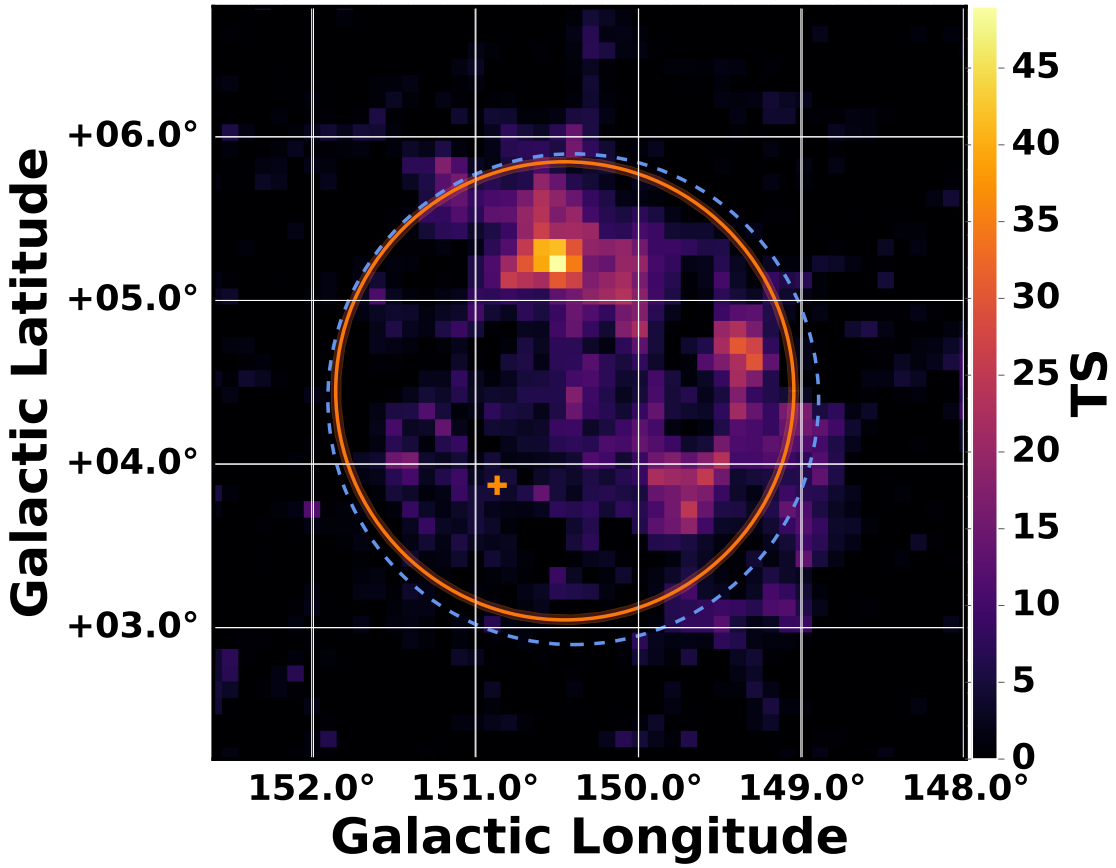

Figure 7.1: Background subtracted residual TS map above 1 GeV with 0.1°x 0.1° pixels for fixed index $\Gamma = 2$, centered on SNR SNR G150.3+4.5. The orange circle and translucent shading show the fit disk radius and 1σ errors, respectively, for the extended source, the orange cross shows the position of 3FGL J0426.7+5437 (included in the background model), and blue dashed circle is the extent of the radio SNR.

sources but both were insignificant when fit on top of the best fit disk. Figure 7.2 is a Residual TS map of the same region as Figure 7.1, but with the disk source included in the background showing that the disk can account well for the emission in the region.

The morphology of the radio emission is suggestive of an elliptical or ring morphology, so an elliptical disk and ring spatial model were tested as well. For the ring model, the fit reduced to a disk with parameters matching those stated above. Using the elliptical model showed a weak improvement over the radially symmetric

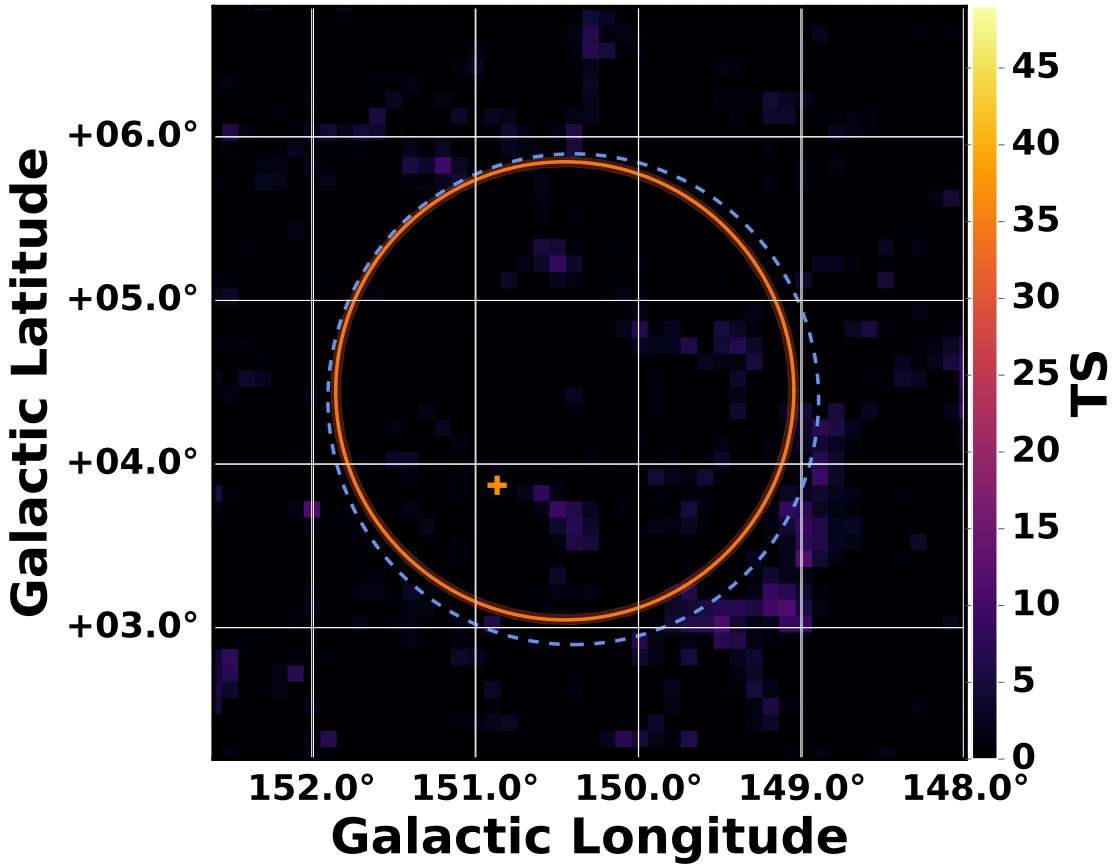

Figure 7.2: Same as Figure 7.1 but with disk in the background model [JAM: should this be a residual counts map instead?]

model at the 2.6σ level ($\Delta\text{TS} = 9$ with two additional degrees of freedom), which we did not consider significant enough to say the GeV emission had an elliptical morphology (see Table **??**). For the remainder of this study, we only considered the disk spatial model.[JAM: put Edisk in table too and reference i.] [JAM: I should double check this for 1GeV- 1TeV. I was done for 1-562 GeV, wait till addSrcs is done]

Other things we tried

fitting an extended source (starting with the 2FHL result) on top of the one currently there. Insignif. idk what to say about 2FHL yet.

another starting at the position of G149. Insignif

Table 7.2. New 2FHL extended sources

Spatial Model [a]	TS	TS_{ext}	σ °	Association	Class	Spatial model	Extension [deg]
J0526.6−6825e	278.843	-32.850	49.80	LMC	gal	2D Gaussian	1.87
J0617.2+2234e	189.048	3.033	398.64	IC 443	snr	2D Gaussian	0.27
J0822.6−4250e	260.317	-3.277	63.87	Puppis A	snr	...	0.37

Note. — This is mostly from 2FHL, just playing with the table. Don't need a table for just disk hypothesis, but maybe to have disk 3 point sources compatison. I tried adding more sources on top of the 3FGL sources and there's no significant residual. where to say something about testing searching for point sources overlapping the extended source and trying to fit an extended source on top as well? in this table give the disk model with best spectral spatial params, TS, TSext dof, LL, then the model with just the 3 3FGL sources (no disk) spectrum of each, TS, dof + LL(didn't relocalize the se sources), separate spatial spectral tables?

[a]comments and notes?

Say something about why we don't just go with the 3 3FGL sources. In the table I shouldn't just compare the 3 to the disk though because I also keep J0426 in the model. So the base comparison is really 2 sources vs the disk. Maybe it's enough to just say of course we keep the disk, we find one at GeV that matches really well with the radio. What did Josh's paper say about how modelling the spectrum of an intrisically extended source as point sources skews the PS spectrum to softer energies?

He said, "Specifically, modeling a spatially extended source as point-like will systematically soften measured spectra", but idk if I get why. We see it with the 2 3FGL sources being softer than what the disk winds up being

Another thing to point out is how modeling as point vs extended, if it's really extended can affect the fit of other point sources nearby, like J0426, so I should show the spectrum of this source too? I fit both the norm and index of the source.

7.2.3 Spectral Analysis

After determining the best fit morphology with `pointlike` for the GeV emission coincident with SNR SNR G150.3+4.5, we used those results as a starting point for our `gtlike` maximum likelihood fit of the region to estimate the best spectral parameters for our model. The LAT data is well described by a power law across the entire energy range with a photon index, $\Gamma = 1.80 \pm 0.04$, and energy flux above 1 GeV of $(7.17 \pm 0.73$ x$10^{-11})$ erg cm^{-2} s^{-1}and TS = 373 [JAM: these are the point-like results, change them when I get the gtlike res]. We tested the γ-ray spectrum of the extended disk for spectral curvature using a log-normal model (Log Parabola), and find no significant deviation from a power law (ΔTS $\sim$ 1).

Still to do

gtlike

Systematics. Bracketing IRFs, alt iem, try varying the extension? still need to be done. Should probably just move this into the spectral section

7.3 Multiwavelength Observations and Analysis

7.3.1 HI

7.3.2 CO?

Do the CO maps add anything?

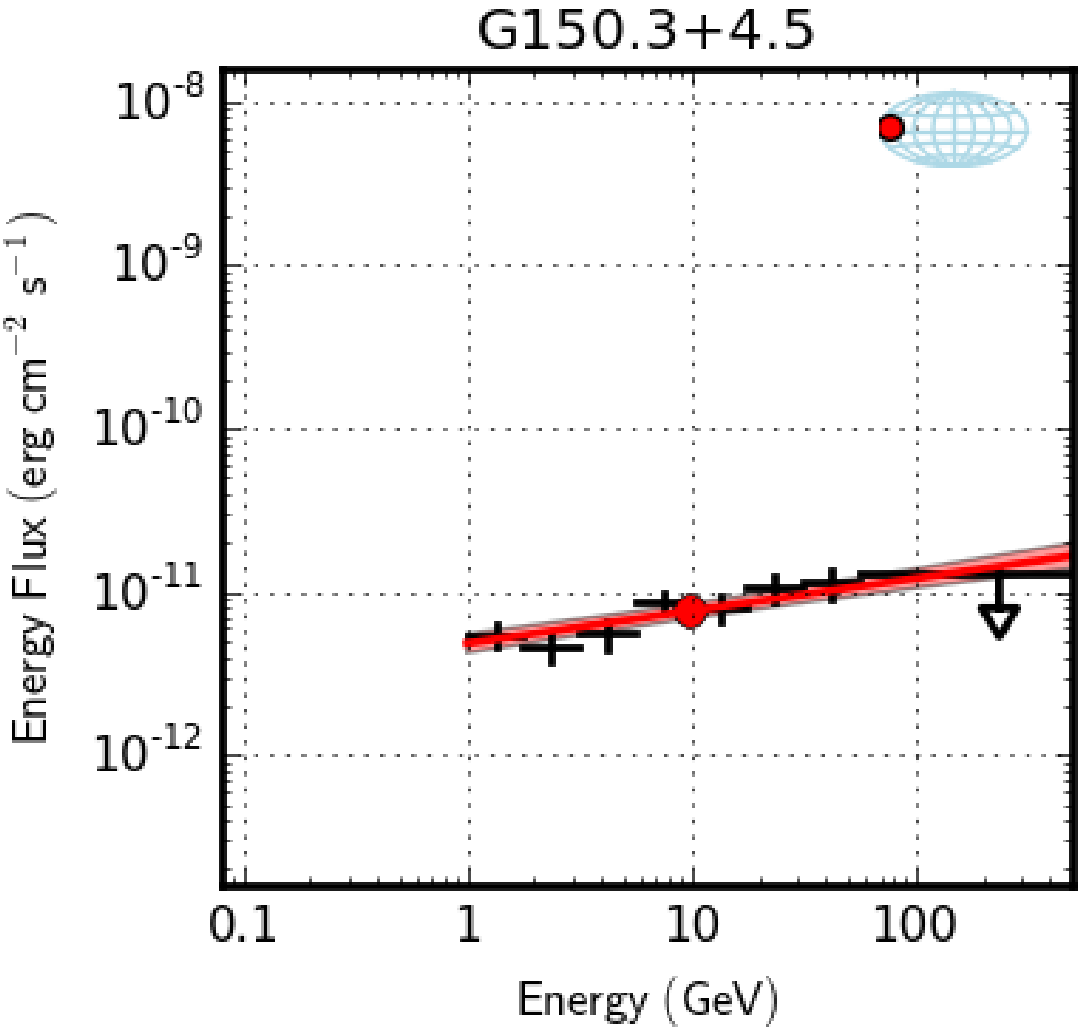

Figure 7.3: Spectral energy distribution for the extended source coincident with SNR SNR G150.3+4.5. [JAM: replace with gtlike SED when I have it]

7.3.3 X-ray

No diffuse nonthermal X-ray emission observed by ROSAT. No point sources near the center? Should a pulsar even be near the center? How to quantify this? Can we place a limit on ambient density with an upper limit on thermal X-ray emission? Magnetic filed with nonthermal?

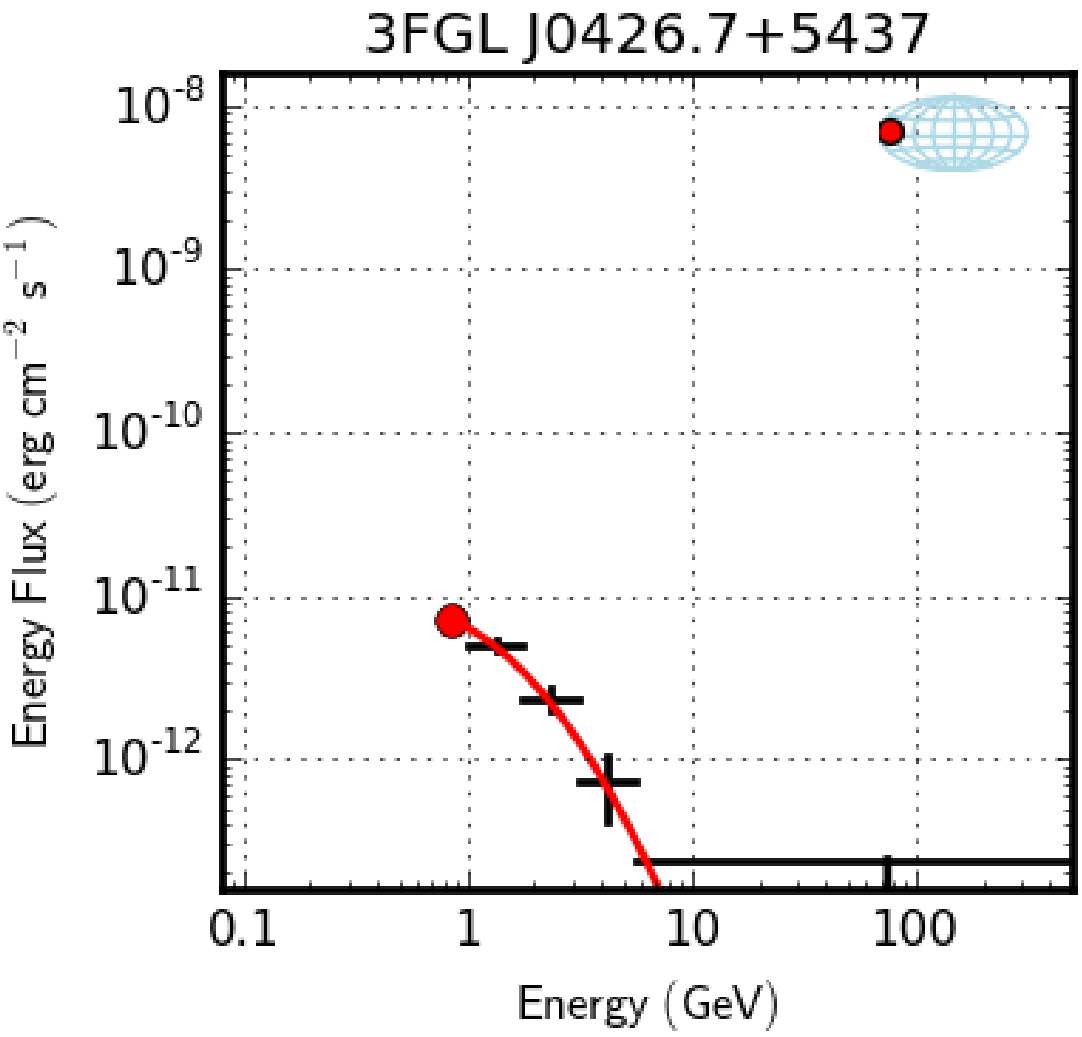

Figure 7.4: Spectral energy distribution of 3FGL J0426.. [JAM: replace with gtlike SED when I have it]

7.4 Discussion and Results

7.4.1 What is it?

Size + HI suggest that near distance corresponding to different HI velocities suggest it's aged, spectrum looks more like young SNR (hard + no GeV break). Is it a weird young remnant or weird aged one? Leptonic dominated if young, hadronic

dominated if older? Something about nearby dense clouds masking hadronic emission? Maybe this is only true for MeV cosmic rays that are screened out though and it would only mask the pion bump, but not this higher energy emission?

PWN or SNR. Can we rule out PWN? See W41 paper, MSH 11-61A, Fabios recent G326 work (no, he just tries to use the PSF types and testing different model templates to try to disentangle SNR from PWN)?

No PSR candidate near center (should it be near the center? Depends on age) Is there some limit we can place on the PWN based on not seeing the pulsar? Like on Edot? OR something like Mattana et al. 2009 correlation between $\mathrm{flux_x}/\mathrm{flux_g} \propto$ Edot?

Assume it's in Sedov phase based on size + near distance, and calculate age, upper limit on Edot base on lack of x-ray flux? Or maybe if I assume the sources is the PWN and GeV radius is PWN radius, then can I estimate Edot based on size and evolution inside SNR?

If we assume close distance, age is only $\approx$ 5kyr, maybe this is a transitional SNR? What do others like this look like? Puppis A? Gamma Cygni is a similar age too.something

7.4.2 Distance Considerations

probably doesn't need to be a different section.

7.4.3 Nonthermal Modeling

I think I could get a working model with naima running pretty quickly, is it worth it?

7.5 Conclusions

[JAM: most of this should be the conclusions from the G150 paper]In this chapter, we have presented the publication on the dedicated analysis of the extended γ -ray emission detected in the direction of SNR G150.3+4.5. SNR G150.3+4.5 was first detected in radio by Gao & Han (2014), and subsequently detected in γ -rays in 2FHLabove 50 GeV. We discussed our LATmorphological analysis at energies E $\geq$ x GeV and spectral analysis down to E $\geq$ 750 MeV, demonstrating a change in extension and centroid position compared to the 2FHLresult. Discuss potential source origin scenarios. Is it SNR or PWN? Is 2FHLsource same as $>$ few GeV?

[JAM: for diss, not paper]. The way this figures into the whole is that this is a follow up analysis of one of the most interesting sources detected with addSrcs, and, (hopefully!), we're able to say something about the source and nature of the γ -ray emission, relation to SNR and 2FHLsource1

Chapter 8

SNR-MC, 10 GeV, and anything else?

Not sure how this is going to factor in yet. supernova remant molecular cloud system (SNR-MC) should fit in somehow since a good deal of work was done? Less certain about 10gev.

Maybe this should say something about how the work I've done has contributed to the field of knowledge but also can lead to future work?

Chapter 9

Conclusions

Finally!

List of Symbols and Acronyms

2FGL Second Fermi LAT source catalog.

2FHL Second Catalog of Hard Fermi-LAT Sources.

2PC Second Fermi LAT catalog of Gamma-ray Pulsars.

AGN active galactic nuclei.

CGRO Compton Gamma-Ray Observatory.

CR cosmic ray.

EGRET Energetic Gamma-Ray Experiment Telescope.

FoV field of view.

GBM Gamma-ray Burst Monitor.

GRB gamma-ray burst.

IC inverse compton.

IEM interstellar emission model.

IRFs instrument response functions.

LAT Large Area Telescope.

LRT likelihood ratio test.

MC molecular cloud.

PL power law.

PSF point spread function.

PWN pulsar wind nebula.

RoI region of interest.

SED spectral energy distribution.

SNR supernova remnant.

SNR-MC supernova remant molecular cloud system.

SNRcat First *Fermi*-LAT Supernova Remnant Catalog.

TS test statistic.

Bibliography

Abdo, A. A. 2009, ArXiv:0902.1340, arXiv:0902.1340:0902.1340

Abdo, A. A., Ackermann, M., Ajello, M., et al. 2009, Science, 325, 840

—. 2010a, ApJS, 188, 405

—. 2010b, ApJ, 722, 1303

—. 2010c, Science, 327, 1103

Abdo, A. A., Ajello, M., Allafort, A., et al. 2013, ApJS, 208, 17

Abramowski, A., Acero, F., Aharonian, F., et al. 2011, A&A, 533, A103

Abramowski, A., Aharonian, F., Ait Benkhali, F., et al. 2015a, A&A, 574, A27

—. 2015b, A&A, 574, A27

Acero, F., Ackermann, M., Ajello, M., et al. 2013, ApJ, 773, 77

—. 2015, ApJS, 218, 23

—. 2016, ApJS, 224, 8

Ackermann, M., Ajello, M., Allafort, A., et al. 2011, Science, 334, 1103

—. 2012a, ApJ, 753, 83

—. 2012b, A&A, 538, A71

Ackermann, M., Ajello, M., Albert, A., et al. 2012c, ApJS, 203, 4

—. 2013, ApJ, 771, 57

Ackermann, M., Ajello, M., Atwood, W. B., et al. 2016, ApJS, 222, 5

Aharonian, F., Akhperjanian, A. G., Bazer-Bachi, A. R., et al. 2006, A&A, 456, 245

Aharonian, F., Akhperjanian, A. G., Barres de Almeida, U., et al. 2008, A&A, 488, 219

Aharonian, F., Akhperjanian, A. G., de Almeida, U. B., et al. 2009, ApJ, 692, 1500

Arzoumanian, Z., Gotthelf, E. V., Ransom, S. M., et al. 2011, ApJ, 739, 39

Atwood, W., Albert, A., Baldini, L., et al. 2013a, ArXiv:1303.3514, arXiv:1303.3514

Atwood, W. B., Abdo, A. A., Ackermann, M., et al. 2009, ApJ, 697, 1071

Atwood, W. B., Baldini, L., Bregeon, J., et al. 2013b, ApJ, 774, 76

Bamba, A., Ueno, M., Koyama, K., & Yamauchi, S. 2001, PASJ, 53, L21

Barr, E. D., Guillemot, L., Champion, D. J., et al. 2013, MNRAS, 429, 1633

Becker, R. H., Markert, T., & Donahue, M. 1985, ApJ, 296, 461

Blair, W. P., Sankrit, R., Torres, S. I., Chayer, P., & Danforth, C. W. 2009, ApJ, 692, 335

Boumis, P., Alikakos, J., Christopoulou, P. E., et al. 2008, A&A, 481, 705

Brogan, C. L., Gelfand, J. D., Gaensler, B. M., Kassim, N. E., & Lazio, T. J. W. 2006, ApJ, 639, L25

Brogan, C. L., & Troland, T. H. 2001, ApJ, 550, 799

Byun, D.-Y., Koo, B.-C., Tatematsu, K., & Sunada, K. 2006, ApJ, 637, 283

Camilo, F., Kaspi, V. M., Lyne, A. G., et al. 2000, ApJ, 541, 367

Camilo, F., Ng, C.-Y., Gaensler, B. M., et al. 2009a, ApJ, 703, L55

Camilo, F., Ransom, S. M., Gaensler, B. M., & Lorimer, D. R. 2009b, ApJ, 700, L34

Camilo, F., Ransom, S. M., Gaensler, B. M., et al. 2006, ApJ, 637, 456

Caraveo, P. A., De Luca, A., Mignani, R. P., & Bignami, G. F. 2001, ApJ, 561, 930

Castelletti, G., Supan, L., Dubner, G., Joshi, B. C., & Surnis, M. P. 2013, A&A, 557, L15

Caswell, J. L. 1985, AJ, 90, 1224

Caswell, J. L., McClure-Griffiths, N. M., & Cheung, M. C. M. 2004, MNRAS, 352, 1405

Caswell, J. L., Murray, J. D., Roger, R. S., Cole, D. J., & Cooke, D. J. 1975, A&A, 45, 239

Chatterjee, S., Brisken, W. F., Vlemmings, W. H. T., et al. 2009, ApJ, 698, 250

Combi, J. A., Albacete Colombo, J. F., Romero, G. E., & Benaglia, P. 2006, ApJ, 653, L41

Combi, J. A., Benaglia, P., Romero, G. E., & Sugizaki, M. 2005, A&A, 431, L9

Dodson, R., Legge, D., Reynolds, J. E., & McCulloch, P. M. 2003, ApJ, 596, 1137

Dubner, G. M., & Arnal, E. M. 1988, A&AS, 75, 363

Eger, P., Rowell, G., Kawamura, A., et al. 2011, A&A, 526, A82

Esposito, J. A., Hunter, S. D., Kanbach, G., & Sreekumar, P. 1996, ApJ, 461, 820

Fesen, R. A., Blair, W. P., & Kirshner, R. P. 1985, ApJ, 292, 29

Frail, D. A., & Clifton, T. R. 1989, ApJ, 336, 854

Frail, D. A., Goss, W. M., Reynoso, E. M., et al. 1996, AJ, 111, 1651

Funk, S., Reimer, O., Torres, D. F., & Hinton, J. A. 2008, ApJ, 679, 1299

Gaensler, B. M., Brazier, K. T. S., Manchester, R. N., Johnston, S., & Green, A. J. 1999, MNRAS, 305, 724

Gaensler, B. M., Fogel, J. K. J., Slane, P. O., et al. 2003, ApJ, 594, L35

Gaensler, B. M., & Wallace, B. J. 2003, ApJ, 594, 326

Gaensler, B. M., Tanna, A., Slane, P. O., et al. 2008, ApJ, 680, L37

Gao, X. Y., & Han, J. L. 2014, A&A, 567, A59

Gerardy, C. L., & Fesen, R. A. 2007, MNRAS, 376, 929

Giacani, E., Smith, M. J. S., Dubner, G., et al. 2009, A&A, 507, 841

Giacani, E. B., Dubner, G. M., Green, A. J., Goss, W. M., & Gaensler, B. M. 2000, AJ, 119, 281

Górski, K. M., Hivon, E., Banday, A. J., et al. 2005, ApJ, 622, 759

Gotthelf, E. V., & Halpern, J. P. 2008, ApJ, 681, 515

Green, D. A. 2004, Bulletin of the Astronomical Society of India, 32, 335

—. 2009, Bulletin of the Astronomical Society of India, 37, 45

Green, D. A. 2012, in American Institute of Physics Conference Series, Vol. 1505, American Institute of Physics Conference Series, ed. F. A. Aharonian, W. Hofmann, & F. M. Rieger, 5–12

—. 2014, Bulletin of the Astronomical Society of India, 42, 47

Green, D. A., Gull, S. F., Tan, S. M., & Simon, A. J. B. 1988, MNRAS, 231, 735

Hailey, C. J., & Craig, W. W. 1994, ApJ, 434, 635

Halpern, J. P., Gotthelf, E. V., & Camilo, F. 2012, ApJ, 753, L14

Harrus, I. M., Hughes, J. P., & Slane, P. O. 1998, ApJ, 499, 273

Hartman, R. C., Bertsch, D. L., Bloom, S. D., et al. 1999, ApJS, 123, 79

Hayato, A., Yamaguchi, H., Tamagawa, T., et al. 2010, ApJ, 725, 894

Helene, O. 1983, Nuclear Instruments and Methods in Physics Research, 212, 319

Hewitt, J. W., Acero, F., Brandt, T. J., et al. 2013, ArXiv e-prints:1307.6570, arXiv:1307.6570

Hewitt, J. W., & Lemoine-Goumard, M. 2015, Comptes Rendus Physique, 16, 674

Hewitt, J. W., Rho, J., Andersen, M., & Reach, W. T. 2009a, ApJ, 694, 1266

Hewitt, J. W., & Yusef-Zadeh, F. 2009, ApJ, 694, L16

Hewitt, J. W., Yusef-Zadeh, F., & Wardle, M. 2008, ApJ, 683, 189

—. 2009b, ApJ, 706, L270

Hewitt, J. W., Yusef-Zadeh, F., Wardle, M., Roberts, D. A., & Kassim, N. E. 2006, ApJ, 652, 1288

Hofverberg, P., Chaves, R. C. G., Fiasson, A., et al. 2010, in 25th Texas Symposium on Relativistic Astrophysics, 196

Inoue, T., Yamazaki, R., & Inutsuka, S.-i. 2010, ApJ, 723, L108

James, F., & Roos, M. 1975, Computer Physics Communications, 10, 343

Jiang, B., Chen, Y., Wang, J., et al. 2010, ApJ, 712, 1147

Johanson, A. K., & Kerton, C. R. 2009, AJ, 138, 1615

Junkes, N., Fuerst, E., & Reich, W. 1992, A&AS, 96, 1

Kassim, N. E., Hertz, P., & Weiler, K. W. 1993, ApJ, 419, 733

Kassim, N. E., & Weiler, K. W. 1990, Nature, 343, 146

Katsuda, S., Tsunemi, H., & Mori, K. 2008, ApJ, 678, L35

Kerr, F. J., & Lynden-Bell, D. 1986, MNRAS, 221, 1023

Kerr, M. 2010, PhD thesis, University of Washington, arXiv:1101.6072

Kim, I.-J., Min, K.-W., Seon, K.-I., Han, W., & Edelstein, J. 2010, ApJ, 709, 823

Koo, B.-C., & Moon, D.-S. 1997, ApJ, 475, 194

Koralesky, B., Frail, D. A., Goss, W. M., Claussen, M. J., & Green, A. J. 1998, AJ, 116, 1323

Kothes, R., & Foster, T. 2012, ApJ, 746, L4

Kothes, R., Reich, W., Foster, T., & Byun, D.-Y. 2003, ApJ, 588, 852

Kothes, R., Uyaniker, B., & Pineault, S. 2001, ApJ, 560, 236

Krause, O., Tanaka, M., Usuda, T., et al. 2008, Nature, 456, 617

Ladouceur, Y., & Pineault, S. 2008, A&A, 490, 197

Lande, J., Ackermann, M., Allafort, A., et al. 2012, ApJ, 756, 5

Landecker, T. L., Pineault, S., Routledge, D., & Vaneldik, J. F. 1989, MNRAS, 237, 277

Lang, C. C., Goss, W. M., Cyganowski, C., & Clubb, K. I. 2010, ApJS, 191, 275

Lazendic, J. S., Wardle, M., Burton, M. G., et al. 2004, MNRAS, 354, 393

Leahy, D., Green, K., & Tian, W. 2014, MNRAS, 438, 1813

Leahy, D., & Tian, W. 2006, A&A, 451, 251

Leahy, D. A., Green, K., & Ranasinghe, S. 2013, MNRAS, 436, 968

Leahy, D. A., & Ranasinghe, S. 2012, MNRAS, 423, 718

Leahy, D. A., & Roger, R. S. 1991, AJ, 101, 1033

Leahy, D. A., Tian, W., & Wang, Q. D. 2008, AJ, 136, 1477

Leahy, D. A., & Tian, W. W. 2007, A&A, 461, 1013

—. 2008a, A&A, 480, L25

—. 2008b, AJ, 135, 167

Lemiere, A., Slane, P., Gaensler, B. M., & Murray, S. 2009, ApJ, 706, 1269

Lemoine-Goumard, M., Renaud, M., Vink, J., et al. 2012, A&A, 545, A28

Lemoine-Goumard, M., Zavlin, V. E., Grondin, M.-H., et al. 2011, A&A, 533, A102

Lopez, L. A., Ramirez-Ruiz, E., Huppenkothen, D., Badenes, C., & Pooley, D. A. 2011, ApJ, 732, 114

Lozinskaya, T. A., Sitnik, T. G., & Pravdikova, V. V. 1993, Astronomy Reports, 37, 240

Malkov, M. A., Diamond, P. H., & Sagdeev, R. Z. 2011, Nature Communications, 2, 194

Massaro, E., Perri, M., Giommi, P., & Nesci, R. 2004, A&A, 413, 489

Mattox, J. R., Bertsch, D. L., Chiang, J., et al. 1996, ApJ, 461, 396

McClure-Griffiths, N. M., Green, A. J., Dickey, J. M., et al. 2001, ApJ, 551, 394

Misanovic, Z., Kargaltsev, O., & Pavlov, G. G. 2010, ApJ, 725, 931

Montmerle, T. 1979, ApJ, 231, 95

Moriguchi, Y., Tamura, K., Tawara, Y., et al. 2005, ApJ, 631, 947

Moriguchi, Y., Yamaguchi, N., Onishi, T., Mizuno, A., & Fukui, Y. 2001, PASJ, 53, 1025

Ng, C.-Y., Romani, R. W., Brisken, W. F., Chatterjee, S., & Kramer, M. 2007, ApJ, 654, 487

Nikolić, S., van de Ven, G., Heng, K., et al. 2013, Science, 340, 45

Nolan, P. L., Abdo, A. A., Ackermann, M., et al. 2012, ApJS, 199, 31

Odegard, N. 1986, ApJ, 301, 813

Ohira, Y., Murase, K., & Yamazaki, R. 2011, MNRAS, 410, 1577

Paron, S., Dubner, G., Reynoso, E., & Rubio, M. 2008, A&A, 480, 439

Paron, S., Ortega, M. E., Rubio, M., & Dubner, G. 2009, A&A, 498, 445

Paron, S. A., Reynoso, E. M., Purcell, C., Dubner, G. M., & Green, A. 2006, PASA, 23, 69

Pauls, T. 1977, A&A, 59, L13

Pfeffermann, E., Aschenbach, B., & Predehl, P. 1991, A&A, 246, L28

Pineault, S., Landecker, T. L., Madore, B., & Gaumont-Guay, S. 1993, AJ, 105, 1060

Prinz, T., & Becker, W. 2012, A&A, 544, A7

Radhakrishnan, V., Goss, W. M., Murray, J. D., & Brooks, J. W. 1972, ApJS, 24, 49

Rakowski, C. E., Badenes, C., Gaensler, B. M., et al. 2006, ApJ, 646, 982

Rakowski, C. E., Hughes, J. P., & Slane, P. 2001, ApJ, 548, 258

Reed, J. E., Hester, J. J., Fabian, A. C., & Winkler, P. F. 1995, ApJ, 440, 706

Reynolds, S. P. 2008, ARA&A, 46, 89

Reynoso, E. M., & Goss, W. M. 1999, AJ, 118, 926

Reynoso, E. M., Green, A. J., Johnston, S., et al. 2004, PASA, 21, 82

Reynoso, E. M., Johnston, S., Green, A. J., & Koribalski, B. S. 2006, MNRAS, 369, 416

Reynoso, E. M., & Mangum, J. G. 2000, ApJ, 545, 874

Roberts, M. S. E., Romani, R. W., Johnston, S., & Green, A. J. 1999, ApJ, 515, 712

Romero, G. E., Benaglia, P., & Torres, D. F. 1999, A&A, 348, 868

Rosado, M., Ambrocio-Cruz, P., Le Coarer, E., & Marcelin, M. 1996a, A&A, 315, 243

—. 1996b, A&A, 315, 243

Routledge, D., Dewdney, P. E., Landecker, T. L., & Vaneldik, J. F. 1991, A&A, 247, 529

Ruiz, M. T., & May, J. 1986, ApJ, 309, 667

Sallmen, S., & Welsh, B. Y. 2004, A&A, 426, 555

Sankrit, R., Blair, W. P., Delaney, T., et al. 2005, Advances in Space Research, 35, 1027

Schwentker, O. 1994, A&A, 286, L47

Sedov, L. I. 1959, Similarity and Dimensional Methods in Mechanics

Seward, F. D., Dame, T. M., Fesen, R. A., & Aschenbach, B. 1995, ApJ, 449, 681

Slane, P., Smith, R. K., Hughes, J. P., & Petre, R. 2002, ApJ, 564, 284

Sollerman, J., Ghavamian, P., Lundqvist, P., & Smith, R. C. 2003a, A&A, 407, 249

—. 2003b, A&A, 407, 249

Stewart, R. T., Caswell, J. L., Haynes, R. F., & Nelson, G. J. 1993, MNRAS, 261, 593

Stupar, M., Parker, Q. A., & Filipović, M. D. 2007, MNRAS, 374, 1441

Sturner, S. J., & Dermer, C. D. 1995, A&A, 293, astro-ph/9409047

Su, Y., Chen, Y., Yang, J., et al. 2011, ApJ, 727, 43

Sun, M., Wang, Z.-r., & Chen, Y. 1999, ApJ, 511, 274

Sun, X. H., Reich, P., Reich, W., et al. 2011, A&A, 536, A83

Tam, P. H. T., Wagner, S. J., Tibolla, O., & Chaves, R. C. G. 2010, A&A, 518, A8

Taylor, G. 1950, Royal Society of London Proceedings Series A, 201, 159

Thompson, D. J., Baldini, L., & Uchiyama, Y. 2012, Astroparticle Physics, 39, 22

Thompson, D. J., Bertsch, D. L., Fichtel, C. E., et al. 1993, ApJS, 86, 629

Tian, W. W., Haverkorn, M., & Zhang, H. Y. 2007a, MNRAS, 378, 1283

Tian, W. W., & Leahy, D. A. 2008a, ApJ, 677, 292

—. 2008b, MNRAS, 391, L54

—. 2011, ApJ, 729, L15

—. 2012, MNRAS, 421, 2593

—. 2013, ApJ, 769, L17

—. 2014, ApJ, 783, L2

Tian, W. W., Leahy, D. A., Haverkorn, M., & Jiang, B. 2008, ApJ, 679, L85

Tian, W. W., Leahy, D. A., & Wang, Q. D. 2007b, A&A, 474, 541

Tian, W. W., Li, Z., Leahy, D. A., & Wang, Q. D. 2007c, ApJ, 657, L25

Tibolla, O. 2009, in American Institute of Physics Conference Series, Vol. 1112, American Institute of Physics Conference Series, ed. D. Bastieri & R. Rando, 211–222

Torres, D. F., Romero, G. E., Dame, T. M., Combi, J. A., & Butt, Y. M. 2003, Phys. Rep., 382, 303

Trimble, V. 1973, PASP, 85, 579

Uchiyama, Y., Funk, S., Katagiri, H., et al. 2012, ApJ, 749, L35

Velázquez, P. F., Dubner, G. M., Goss, W. M., & Green, A. J. 2002, AJ, 124, 2145

Vink, J. 2004, ApJ, 604, 693

Walker, A. J., & Zealey, W. J. 2001, MNRAS, 325, 287

Welsh, B. Y., Sallmen, S., Jelinsky, S., & Lallement, R. 2003, A&A, 403, 605

Xiao, L., & Zhu, M. 2012, A&A, 545, A86

Xilouris, K. M., Papamastorakis, J., Paleologou, E. V., Andredakis, Y., & Haerendel, G. 1993, A&A, 270, 393

Yamaguchi, H., Ueno, M., Koyama, K., Bamba, A., & Yamauchi, S. 2004, PASJ,

56, 1059

Yar-Uyaniker, A., Uyaniker, B., & Kothes, R. 2004, ApJ, 616, 247

Yusef-Zadeh, F., Goss, W. M., Roberts, D. A., Robinson, B., & Frail, D. A. 1999, ApJ, 527, 172

Yusef-Zadeh, F., Arendt, R. G., Heinke, C. O., et al. 2007, in IAU Symposium, Vol. 242, IAU Symposium, ed. J. M. Chapman & W. A. Baan, 366–373

Zhou, P., & Chen, Y. 2011, ApJ, 743, 4

Zhou, X., Chen, Y., Su, Y., & Yang, J. 2009, ApJ, 691, 516

Zhu, H., Tian, W. W., Torres, D. F., Pedaletti, G., & Su, H. Q. 2013, ApJ, 775, 95